MILLING FORCE ESTIMATION USING ANGULAR DOMAIN HARMONICS WITH KALMAN FILTER USING ACCELERATION DATA

A THESIS SUBMITTED TO
THE GRADUATE SCHOOL OF NATURAL AND APPLIED SCIENCES
OF
MIDDLE EAST TECHNICAL UNIVERSITY

BY

MERT İLME

IN PARTIAL FULFILLMENT OF THE REQUIREMENTS
FOR
THE DEGREE OF MASTER OF SCIENCE
IN
MECHANICAL ENGINEERING

NOVEMBER 2024

Approval of the thesis:

MILLING FORCE ESTIMATION USING ANGULAR DOMAIN HARMONICS WITH KALMAN FILTER USING ACCELERATION DATA

submitted by **MERT İLME** in partial fulfillment of the requirements for the degree of **Master of Science in Mechanical Engineering Department, Middle East Technical University** by,

Prof. Dr. Naci Emre Altun
Dean, Graduate School of **Natural and Applied Sciences** _____

Prof. Dr. Serkan Dağ
Head of Department, **Mechanical Engineering** _____

Assist. Prof. Dr. Hakan Çalışkan
Supervisor, **Mechanical Engineering, METU** _____

Prof. Dr. R. Tuna Balkan
Co-supervisor, **Mechanical Engineering, METU** _____

Examining Committee Members:

Assoc. Prof. Dr. Ulaş Yaman
Mechanical Engineering, METU _____

Assist. Prof. Dr. Hakan Çalışkan
Mechanical Engineering, METU _____

Assoc. Prof. Dr. Ender Yıldırım
Mechanical Engineering, METU _____

Assist. Prof. Dr. Orkun Özşahin
Mechanical Engineering, METU _____

Assist. Prof. Dr. R. Hakkı Namlu
Mechanical Engineering, Atılım University _____

Date: 28.11.2024

I hereby declare that all information in this document has been obtained and presented in accordance with academic rules and ethical conduct. I also declare that, as required by these rules and conduct, I have fully cited and referenced all material and results that are not original to this work.

Name, Surname: Mert İlme

Signature :

ABSTRACT

MILLING FORCE ESTIMATION USING ANGULAR DOMAIN HARMONICS WITH KALMAN FILTER USING ACCELERATION DATA

İlme, Mert
M.S., Department of Mechanical Engineering
Supervisor: Assist. Prof. Dr. Hakan Çalışkan
Co-Supervisor: Prof. Dr. R. Tuna Balkan

November 2024, 82 pages

In order to make a contribution to the Industry 4.0 concept, today's milling research is mainly focusing on the identification of the cutting process. To identify the cutting process, it is vital to know the cutting forces. Since directly measuring the force is costly and inconvenient, there is a need for a simpler way to indirectly estimate the cutting forces. In this thesis, a novel model-based estimation algorithm using the acceleration data is proposed. The model is based on a angular domain force model which consists of the harmonics at the orders of the tooth passing frequency. The force model is converted into the acceleration model by the frequency response function of the workpiece. The acceleration model is integrated into the Kalman filter. With the measured acceleration feedback, the Kalman filter estimates the cutting force. The proposed method is verified with experimental data.

Keywords: Milling, Cutting Force Estimation , Kalman Filtering

ÖZ

AÇISAL ALAN HARMONİKLERİ İLE FREZELEME KUVVETLERİNİN İVME VERİSİ KULLANILARAK KALMAN FİLTRE İLE TAHMİN EDİLMESİ

İlme, Mert
Yüksek Lisans, Makina Mühendisliği Bölümü
Tez Yöneticisi: Dr. Öğr. Üyesi. Hakan Çalışkan
Ortak Tez Yöneticisi: Prof. Dr. R. Tuna Balkan

Kasım 2024 , 82 sayfa

Endüstri 4.0 konseptine katkı sağlamak amacıyla, günümüzde frezeleme araştırmaları ağırlıklı olarak kesme sürecinin tanımlanmasına odaklanmaktadır. Kesme sürecini tanımlamak için kesme kuvvetlerini bilmek kritik öneme sahiptir. Kuvvetin doğrudan ölçülmesi maliyetli ve zahmetli olduğundan, kesme kuvvetlerini dolaylı olarak tahmin edebilecek daha basit bir yönteme ihtiyaç vardır. Bu tezde, ivme verilerini kullanarak yeni bir model tabanlı tahmin algoritması önerilmektedir. Model, diş geçiş frekansı harmoniklerini içeren açısal alan kuvvet modeline dayanmaktadır. Kuvvet modeli, iş parçasının frekans tepki fonksiyonu ile ivme modeline dönüştürülmüştür. İvme modeli, Kalman filtresine entegre edilmiştir. Ölçülen ivme geri bildirimi ile Kalman filtresi kesme kuvvetini tahmin etmektedir. Önerilen yöntem, deneysel verilerle doğrulanmıştır.

Anahtar Kelimeler: Frezeleme, Kesme Kuvveti Tahmini, Kalman Filtre

To my family,

ACKNOWLEDGMENTS

The author wishes to express his deepest gratitude to his supervisor Assist. Prof. Dr. Hakan Çalışkan and co-supervisor Prof. Dr. Tuna Balkan for their guidance, advice, criticism, encouragements and insight throughout the research.

The author would also like to thank Assist. Prof. Dr. Orkun Özşahin for his suggestions and comments.

The technical assistance of Mr. Barış Altun is gratefully acknowledged.

This work is partially funded by ODTÜ BAP under grant number ADEP-302-2023-11219.

TABLE OF CONTENTS

LIST OF TABLES

TABLES

LIST OF FIGURES

FIGURES

LIST OF ABBREVIATIONS

AI	Artificial Intelligence
CNC	Computer Numerical Control
CWD	Chip Width Density
DC	Direct Current
FEM	Finite Element Method
FRF	Frequency Response Function
FFT	Fast Fourier Transform
IFFT	Inverse Fast Fourier Transform
IoT	Internet of Things
ML	Machine Learning
RMS	Root Mean Square
SVD	Singular Value Decomposition
TSVD	Truncated Singular Value Decomposition
WP	Workpiece

LIST OF SYMBOLS

a_0, a_k, b_k	Coefficients of Fourier Series Expansion
$A_0^{p_1}, A_k^{p_1}, B_k^{p_1}$	Coefficients of Fourier Series Expansion for p_1 Function
a_e	Radial Depth of Cut
a_p	Axial Depth of Cut
b_h	Tool Geometry Factor
$d\beta$	Angular Increment of Cutter
dz	Axial Increment
D	Diameter of Cutting Tool
f_a	Axial Cutting Force
f_t	Tangential Cutting Force
f_r	Radial Cutting Force
f_x, f_y, f_z	X, Y and Z Components of Cutting Force
k_a	Axial Cutting Ratio
k_t, K_t	Tangential Cutting Coefficient
k_r	Radial Cutting Ratio
K_r	Radial Cutting Coefficient
k_{te}, K_{te}	Tangential Edge Coefficient
k_{re}	Radial Edge Ratio
K_{re}	Radial Edge Coefficient
K	Cutting Coefficient Matrix
K_4	Cutting and Edge Coefficients Matrix
N	Number of Teeth
p_1, p_2, p_3	Components of Elementary Cutting Functions

p_x, p_y, p_z	X, Y and Z Elementary Cutting Functions
q	Number of Harmonics
R	Radius of Cutting Tool
t_c	Average Chip Thickness
t_x	Feed Rate per Tooth
$w(\theta)$	Window Function of Engagement
α	Helix Angle of Cutting Tool
β	Angle of Cutter from Flute Tip
β_0	Axial Engagement Angle
θ	Angle of Cutting Tool Tip
θ_1, θ_{st}	Entering Angle of Cutting Tool into Workpiece
θ_2, θ_{ex}	Exiting Angle of Cutting Tool from Workpiece
ϕ	Spindle Angle
$\dot{\phi}$	Spindle Speed

CHAPTER 1

INTRODUCTION

The growing demand for raw materials, driven by increasing production and consumption, has made their efficient use essential in the manufacturing industries. To improve the efficiency, production processes have been digitized through technologies such as the Internet of Things (IoT), Artificial Intelligence (AI), Big Data Management, collectively known as Industry 4.0. These advancements transform machines into intelligent systems capable of autonomous analysis and decision-making, leading to more efficient production, fewer errors, and reduced costs.

In the manufacturing field of production, milling is one of the most common machining method. Current research in milling focuses on controlling the cutting process to achieve benefits such as extended tool life, reduced tool and tool change costs, controlled vibration and noise levels, and health monitoring to minimize maintenance issues. Controlling the cutting process also enhances surface finish quality and gives the ability to optimize the parameters for an efficient and safe process. Understanding the cutting forces in milling, which consist of tangential, radial, and axial components, is essential for achieving those benefits. The most guaranteed way to obtain the cutting forces is measuring them using dynamometers, or piezoelectric force sensors which is known for their high accuracies and high bandwidths but it is known that those measuring devices are costly. They often need special arrangements in terms of mounting issues. Installing all the production line with dynamometers would be challenging due to those reasons. As a result, there is a need for more straightforward and more cost-effective ways to monitor cutting forces and milling conditions. Instead of directly measuring the force, it can be found by making estimations using other data in the system. Today's sensor technology and computational techniques are capable

of offering precise and cost-effective solutions using sensor data. Therefore, in this thesis, it is aimed to find a simpler, cost-effective indirect force estimation method using other sensor data.

1.1 Literature Review

There are several approaches used in the literature to make a force estimation. They differ from each other by the measured data and the estimation algorithm developed. The mostly used data is the acceleration data measured with accelerometers. They provide high bandwidth, simplicity in mounting and data processing. In the other works, capacitive displacement sensors are used in addition to the accelerometers. Some other researchers tried to use servo-data of the CNC such as feed torque or feed current etc. and end up with low bandwidth solutions. Furthermore, it is shown that the motor drive current can also be used to estimate the cutting forces. In this thesis, due to their advantages over the others, the accelerometers are preferred for the estimation process. In the acceleration-based estimation algorithms worked on in the literature, the base mathematical model is the vibration model of the workpiece or the spindle box. However, in this thesis, a force model is directly used in the basis of calculations and is converted into the acceleration model. Therefore, a force model is needed in this thesis. Before the estimation algorithm, the literature is scanned for a suitable force model which can be properly related with acceleration and applicable to an estimation algorithm.

1.1.1 Force Models

For the cutting force model in milling process, there exist different approaches in the literature. Traditionally, in the first years of milling force modelling, Boston et al. [1], Armarego and Brown [2] found an experimental way in which the basic process variables are correlated with average force components. After Martellotti [3] revealed that average chip thickness oscillates depending on cutter rotation ,the chip formation model made popular to use semi-empirical and mechanistic models. Koenigsberger and Sabberwal [4] extended Martellotti's assumption by including factors of tool and

workpiece properties and improved its accuracy. Kline et al. [5] proposed a mechanistic model that calculates the cutting forces by separating the components of cutting force into tangential, radial, and axial components based on chip thickness and cutting coefficients which are decided empirically. In [6-8], the force is calculated with convolution multiplication of basic cutting functions. The cutting coefficients are empirically obtained. In those models, the harmonics of the cutting forces are acquired and are available to be converted into time or angular domain. The basic cutting functions simplify the force expression into the process parameters such as cutter geometry, axial and radial depth of cut, spindle speed and feed rate. However, these semi-empirical mechanistic models needs new preliminary experiments to decide cutting coefficients for new cutters which makes them unuseful for different and complex geometries as mentioned by Yucesan and Altintas [9]. Alternatively, there exists force models depending on the mechanics of orthogonal cutting. Armarego and Uthaichaya [10] and Altintas and Budak [11] use basic cutting properties from orthogonal cutting tests to create a common database adaptable to different tool geometries and scenarios. This orthogonal database is then used for different cutting operations with kinematic transformations.

Although they are out of scope of this thesis since no mathematical expression is included, with the help of computational power, FEM-based models are used to obtain the cutting force by Movahhedy et al. [12]. In those models, temperature and stress issues can be examined in details. Lastly, Zhu et al. [13] and Khan et al. (2020) [14] used artificial intelligence (AI) and machine learning (ML) approaches to find forces in cutting process. Since they are computationally expensive, their usage is limited.

After examining the different approaches for force models in the literature, the most useful method that suits best to the aim of this thesis is the convolution models developed as in [6-8]. Their simplicity and the flexibility in tuning the cutting coefficients are the main reasons to move on with those works. The mathematical structure of them will be discussed in the following chapters.

1.1.2 Estimation of Cutting Forces and Coefficients

For the estimation model there are several approaches in the literature. In plenty of researches, regression methods are used. This statistical method is advantageous when unknown dynamics exist in the system. It needs sufficient data to train or to model the system. It may need recalibration for changing parameters. Next, some decomposition methods are preferred when the signal is needed to be decomposed into its components. It provides to work in frequency domain. Singular value decomposition or Fourier transform are the common type of decomposition methods. There exists regularization methods in order to get over the ill-conditioned situation due to DC component between acceleration and force like Tikhonov regularization. Lastly, the most common estimation method is the observer-based methods. The Kalman filter is widely used for that purpose which gives the ability to make real-time estimations and to satisfy robustness against the discrepancies in the system. For the conversion from the measured data to force, a transformation method is needed. For this purpose, the frequency response function of the dynamic system which is obtained by utilizing a modal test is used. Depending on the transformed data, some algebraic equations are also used in some cases.

In [15], Kakkassery and Uthayakumar used the measurements from servo-controller of the machine. They collect the motor drive current and some CNC measurements such as position, speed and torque and by removing the feed dynamics using frequency response they estimate the force. At the end, they concluded their work as a simpler approach with less bandwidth and accuracy compared to direct measurement of force. In [16], Albertelli et al. used multiple sensors which are accelerometers and displacement sensors mounted in the workpiece and spindle in order to estimate the cutting forces and tool tip vibrations to check the surface quality. As the estimator, they developed a model-based one according to the Kalman filter. In [17], Kıran and Kayacan aimed to find the cutting force for flexible parts such as thin walled pieces by measuring the dynamic force and eliminating the dynamics with inverse filtering. The similar work is done by Altıntaş [18], making force to force identification between tool tip and force sensor integrated in spindle. Using Kalman filter, structural modes are aimed to be filtered and undistorted force is found. In [19], Li et al. made force

estimation using accelerometers mounted on the spindle box. They used Tikhonov regularization method which they improved to decrease the process time for estimations. In their work, it is mentioned that considerable research has been done for force identification however the important point is about process time without decreasing the accuracy. In [20], Wang et al. used accelerometers mounted on spindle box to estimate the force. For the estimator, truncated singular value decomposition (TSVD) method is applied. In [21], Zhou et al. designed a Kalman filter with the vibration acceleration for dynamic cutting force. For the static component of force, they used a displacement sensor mounted on the spindle. In [22], Patil and Gombi estimated the force using acceleration data with singular value decomposition (SVD) method. In [23], Joddar and Ahmadi estimated the force using the Augmented Kalman filter with the vibration model of the workpiece. In [24], Powalka et al. made force estimation with accelerometer and Tikhonov regularization technique. In [25], Kouguchi and Yoshioka eliminated high frequency components of acceleration with an approximation of sequential quadratic regression method. With the vibration model of the spindle box, the force is estimated. In [26], authors used spindle acceleration and motor current data to estimate the cutting forces.

After examining the different approaches for estimation algorithms used in the literature, the most useful method that provides the simplicity and accordance to the aim of the thesis is chosen to be the observer-based Kalman filter method. Its simplicity and the flexibility combined with the force model in tuning the cutting coefficients are the main reasons to move on with the Kalman filter. The mathematical structure will be discussed in the following chapters.

1.2 Scope of the Thesis

Overall, in the literature, the most common method to estimate the cutting force is seen as using the vibration data measured with accelerometers. The main reasons beyond the accelerometer preference are mainly the simplicity of them in terms of mounting and data collection, and higher bandwidth compared to CNC or motor drive data. In this thesis, accelerometer mounted on the workpiece is used for force estimation.

In the literature, the acceleration signal is commonly processed to eliminate the unnecessary components and the vibration model is obtained by an impact test. The vibrational characteristics of the spindle or workpiece is included in the estimation algorithms. The transfer matrix between acceleration and milling force is usually ill-conditioned. The common challenge in the previous work is about finding the DC or low-frequency components of the force since the piezoelectric accelerometers are not suitable for static measurement of the acceleration. This ill-condition is mostly solved by regularization algorithms in the literature. Authors made improvements on their algorithms to achieve the static component of the force accurately. Regularization algorithms are straightforward and quick to implement providing a direct relation between acceleration and force. They have low computational costs, however in complex conditions their ability is limited. For changing or non-linear conditions they need recalibration. In order to have more accurate estimation algorithm, the observer-based estimation algorithms could be chosen. It requires an accurate process model. Although they would be robust against smaller modelling errors and noises, some discrepancies might cause poor performance. For more robust estimation, the Kalman filter could be adapted to the process. It would behave more flexible to the discrepancies. However, for the Kalman filter structure, an accurate process and a measurement model should be constructed. In addition, those models should not be very complex to avoid process time. In this thesis, the existing methodologies for estimating cutting forces with acceleration data is reviewed and the advantages of different estimation methods tried to be joined together. The simplicity of regularization methods, the accuracy of observer-based models and the flexibility of Kalman filter are collected in this work. In the thesis, acceleration is chosen to be used as the measured data to estimate the cutting force. For this purpose, an accelerometer is mounted on the workpiece. One novel part of this work different from the literature is that the force is not estimated using the vibration model. A force model is directly used in the basis of calculations for robustness and accuracy. For the force model, Zheng et al.'s "Angle Domain Analytical Model for End Milling Forces" [8] is chosen. This model offers a simple structured, precise, adaptable, and computationally efficient way to calculate cutting force. Most importantly, it provides the harmonics of the cutting forces in tooth passing frequencies as a function of cutter angle. It is already known that the force harmonics occur in the tooth passing frequencies in

case of no run-out. Using that fact, unnecessary calculations and transfer function estimations can be neglected. Since a force model is used in the algorithm, no additional work is needed for mean value estimation of force. Moreover, it provides flexibility in tuning and including the cutting coefficients in the calculations. These benefits make this force model particularly valuable to be used in estimation algorithm. This force model was constructed with two cutting coefficients. In this thesis, two edge coefficients are added to the force model to increase the accuracy as a novelty. Next, to reflect the vibration characteristics of the workpiece, an impact hammer test is performed. Instead of using transfer function identification or reverse filtering algorithms to relate the force with acceleration as in the literature, the force model makes it available to convert the force harmonics to the acceleration harmonics with basic mathematical operations. Using the results of the modal test, the gains are multiplied and the phases are added to the force harmonics at tooth passing frequencies and the acceleration harmonics can be found with less computational work. The acceleration model is rearranged and adapted for the Kalman filter structure. The states of the Kalman is chosen to be the cutting coefficients only. The measurement matrix of Kalman consists of the multiplicators of acceleration harmonics. No discrete conversion of transfer functions is needed in the Kalman. The Kalman output gives the acceleration in angular domain. Running the Kalman filter with process and measurement data, the cutting coefficients are adjusted by Kalman and the cutting force is estimated using acceleration measurement for a specific cutter angle. The schematic representation of the algorithm can be seen on Fig. 1.1.

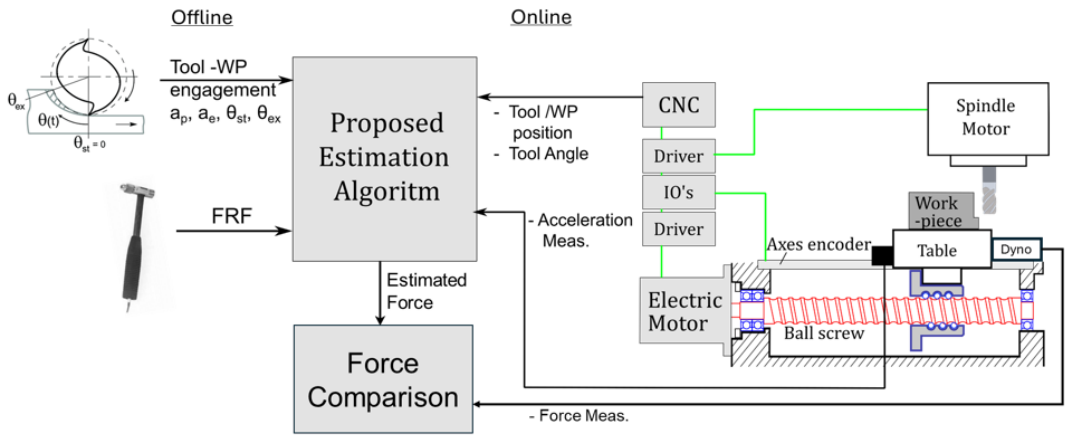

Figure 1.1: Schematic Representation of the Proposed Algorithm

The work is divided into two parts which are online and offline parts. The cutting tests and data collection is the online part. Acceleration, tool angle and position, force data are collected online. After, the estimation part using the data is the offline part. Axial (a_p) and radial (a_e) depth of cut, entrance (θ_{st}) and exit (θ_{ex}) angles and FRF results are processed with the algorithm after the tests. The algorithm is suitable for online identification, however it is planned as future work for now. The algorithm is supported with numerical simulations and experimental tests at the end. The results seem to be satisfying. By enhancing the understanding of milling forces, the study aims to contribute to the literature with a novel force-model based estimation algorithm consisting of two cutting and two edge coefficients for indirect estimation of cutting force in milling using acceleration measurement. With the work, it is aimed to improve manufacturing efficiency, reduce environmental impact, and lower the manufacturing costs. The structure of the thesis is as follows.

In Chapter 1, a review of the existing methodologies in the literature is presented. In order to use acceleration to reach the force, a force model has to be used in the basis of the algorithm. Different approaches for force expressions are discussed. After, the force should be related to the acceleration. Further acceleration mappings are reviewed in the chapter. Generally, these methods are based on the vibration model of the workpiece. Various milling force estimation models developed by different authors are discussed. Finally, the estimation algorithm developed in this thesis is compared with the literature work. A summary of the work is given.

In Chapter 2, the main force model used in this thesis is explained. The steps of the force model derivation is given. Additionally, in this thesis, an improvement on the force model is done to get more accurate force expression. The details and the derivation of improved part is also clarified. To validate the improvement for increasing the accuracy, a cutting test is planned to compare the original force expression with improved one and the real cutting forces. The results are compared and necessity of the improvement on the force model is expressed.

In Chapter 3, an explanation is given about how the estimation algorithm is developed. In previous chapter, the force model was derived. In this chapter, the force model is combined with the workpiece dynamics and an expression for the acceleration model

is established. The conversion from force to acceleration is done by using the force harmonics and the frequency response gains and phases in each relevant frequencies. The acceleration expression is obtained as a harmonic sum. By rearranging the acceleration expression, the system model is stated. Next, the Kalman structure expressed. To validate the estimation algorithm and Kalman structure mathematically, a simulation model is constructed in Matlab/Simulink. The results are discussed and the important points about the algorithm is clarified.

In Chapter 4, mathematically verified algorithm is tried in real cutting tests. Test setup is introduced and various test scenarios in different configurations are planned. After the real cutting tests, the results are discussed. They are compared with each other.

In the last Chapter 5, an overall conclusion is done. The method, test results, their accuracies and precisions are evaluated. The advantages and disadvantages compared with other methods are discussed. The accuracies are debated with roots and causes. Lastly, the possible improvements that can be made as a future work to the proposed method is examined.

The proposed method offers substantial potential for improving milling process monitoring and control without relying on direct force sensors. The approach could be integrated into adaptive control systems, enhancing milling precision and extending tool life. This study marks progress toward developing more flexible, sensor-efficient solutions for milling applications.

CHAPTER 2

MILLING FORCE MODEL

In milling, the tool is fed towards the workpiece. When one of the cutting edge of the tool penetrates into the workpiece, a resistive contact force starts to rise which is called the cutting force. In Fig. 2.1, the representation of the cutting tool and workpiece interaction can be seen. X is assumed as the feed direction. Z is the axial direction of the cutting tool. The tangential cutting force occurs at the point that the cutting edge touches the workpiece in the tangent direction. The radial cutting force occurs at the normal direction inline with the touching point and cutter center. The axial force occurs at the Z direction. ϕ is the absolute spindle angle, which can be noted as the angular position of any cutting edge with respect to any reference. θ is the angular position of any cutting point with respect to same reference as ϕ. β is the angular position of that cutting point with respect to the relevant cutting edge tip. The derivation of force expression is done according to the given variables and coordinate systems.

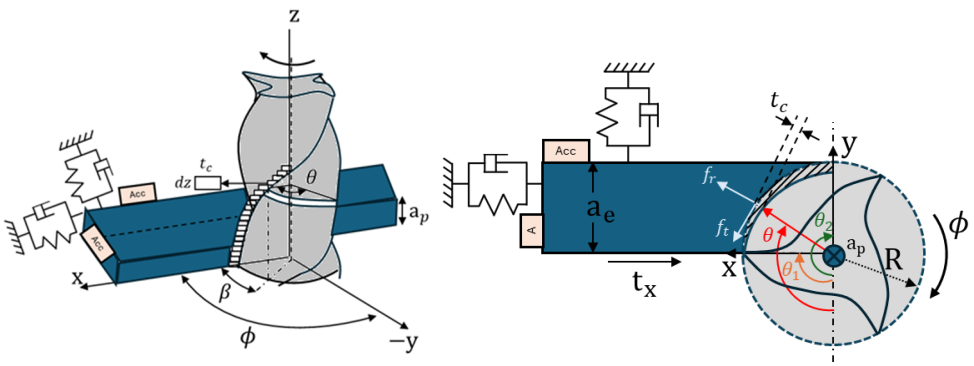

(a) Isometric View (b) Top View

Figure 2.1: One Flute Cutting Forces

The force models in the literature are based on the relation between cutter and chip thickness which is expressed by Martelotti [3], where t_c is average chip thickness, and t_x feed per tooth and θ cutter position. It is mentioned as a good approximation in the literature.

$$t_c = t_x \cdot sin\theta \tag{2.1}$$

Koenigsberger and Sabberwal [4] suggested that local tangential cutting force can be expressed in terms of average chip thickness.

$$f_t(\theta) = k_t \cdot t_c(dz) = k_t \cdot t_x sin\theta(dz) \tag{2.2}$$

As shown in Figure 2.1, (dz) is the infinitesimal chip width, k_t is empirically determined tangential cutting coefficient. In order to reflect whether the cutter is in workpiece or not, a window function is described. θ_1 and θ_2 are entrance and exit angles of cutter. 2.2 is combined with window function.

$$w(\theta) = 1 \quad for \quad \theta_1 \leq \theta \leq \theta_2; \quad w(\theta) = 0 \quad otherwise$$

$$f_t(\theta) = k_t \cdot t_c(dz) = k_t \cdot t_x sin\theta(dz) \cdot w(\theta) \tag{2.3}$$

Tlusty and MacNeil [27] and Fu et al. [28] related the radial and axial cutting forces to tangential cutting force using cutting ratios.

$$f_r(\theta) = k_r \cdot f_t, \quad f_a(\theta) = k_a \cdot f_t \tag{2.4}$$

Based on the coordinate system as in Figure 2.1, the tangential, radial and axial forces are transformed into rectangular coordinate system.

$$\begin{pmatrix} f_x(\theta) \\ f_y(\theta) \\ f_z(\theta) \end{pmatrix} = \begin{pmatrix} cos\theta & sin\theta & 0 \\ sin\theta & -cos\theta & 0 \\ 0 & 0 & 1 \end{pmatrix} \begin{pmatrix} f_t(\theta) \\ f_r(\theta) \\ f_a(\theta) \end{pmatrix} \tag{2.5}$$

The local cutting forces expressed in Eqn. 2.5 are normalized with maximum tangential cutting force ($f_t = k_t t_x$) to obtain the elementary cutting forces p_x, p_y, p_z which gives the cutting forces on unit cutting area.

$$\begin{pmatrix} p_x(\theta) \\ p_y(\theta) \\ p_z(\theta) \end{pmatrix} = \frac{1}{k_t \cdot t_x(dz)} \begin{pmatrix} f_x(\theta) \\ f_y(\theta) \\ f_z(\theta) \end{pmatrix} \tag{2.6}$$

Eqn. (2.3-2.6) can be rearranged that:

$$\begin{pmatrix} p_x(\theta) \\ p_y(\theta) \\ p_z(\theta) \end{pmatrix} = \begin{pmatrix} 1 & k_r & 0 \\ -k_r & 1 & 0 \\ 0 & 0 & k_a \end{pmatrix} \begin{pmatrix} p_1(\theta) \\ p_2(\theta) \\ p_3(\theta) \end{pmatrix} \tag{2.7}$$

where

$$p_1(\theta) = \frac{1}{2} \cdot sin(2\theta) \cdot w(\theta), \quad p_2(\theta) = \frac{1}{2} \cdot (1 - cos(2\theta)) \cdot w(\theta), \quad p_3(\theta) = sin(\theta) \cdot w(\theta)$$

The derived force equations are cutting forces for a unit area of $t_c \cdot dz$. Total cutting force can be found with the integration along the entire cutting flute.

$$\begin{pmatrix} f_x(\phi) \\ f_y(\phi) \\ f_z(\phi) \end{pmatrix} = \int_0^{\phi} \begin{pmatrix} \bar{f}_x(\theta) \\ \bar{f}_y(\theta) \\ \bar{f}_z(\theta) \end{pmatrix} \tag{2.8}$$

Combining Eqn. 2.6, 2.7 and 2.8, total cutting forces can be rewritten with the relation $\theta = \phi - \beta$ where β is the angular position of the cutting point with respect to its flute tip.

$$\begin{pmatrix} f_x(\phi) \\ f_y(\phi) \\ f_z(\phi) \end{pmatrix} = k_t \cdot t_x \begin{pmatrix} 1 & k_r & 0 \\ -k_r & 1 & 0 \\ 0 & 0 & k_a \end{pmatrix} \int_0^{\phi} \begin{pmatrix} p_1(\phi - \beta) \\ p_2(\phi - \beta) \\ p_3(\phi - \beta) \end{pmatrix} dz \tag{2.9}$$

The axial increment (dz) should be related with the rotation of cutting flute. It can be rewritten in terms of β as:

$$dz = b_h \cdot d\beta \quad where \quad b_h = \frac{R}{tan(\alpha)} \quad for \quad 0 \leq \beta \leq \frac{a_p \cdot tan(\alpha)}{R}; \quad 0 \quad otherwise \tag{2.10}$$

where b_h is the tool geometry factor which gives the idea whether the cutting tool edge is axially in contact with the workpiece or not, R is the cutter radius, α is the

helix angle of cutter, a_p is the axial depth of cut. By substituting Eqn. 2.10 into Eqn. 2.9 the total force expression could be derived for single tooth only. Including the N cutting flutes to the force expression, the total cutting force can be rewritten as the following equation.

$$\begin{pmatrix} f_x(\theta) \\ f_y(\theta) \\ f_z(\theta) \end{pmatrix} = k_t \cdot K \cdot t_x \cdot b_h \sum_{m=0}^{N-1} \int_{2m\pi/N}^{2m\pi/N+\beta_0} \begin{pmatrix} p_1(\theta) \\ p_2(\theta) \\ p_3(\theta) \end{pmatrix} \cdot w(\theta) \cdot d\beta \tag{2.11}$$

in which

$$K = \begin{bmatrix} 1 & k_r & 0 \\ -k_r & 1 & 0 \\ 0 & 0 & k_a \end{bmatrix}, \quad \begin{bmatrix} p_1(\theta) \\ p_2(\theta) \\ p_3(\theta) \end{bmatrix} = \begin{bmatrix} \frac{\sin 2\theta}{2} \\ \frac{1-\cos 2\theta}{2} \\ \sin\theta \end{bmatrix}, b_h = \frac{R}{\tan\alpha}, \quad \beta_0 = \frac{a_p \tan\alpha}{R}, \tag{2.12}$$

$$w(\theta) = \begin{cases} 1, & \text{for } 2\pi k + \theta_1 < \theta < 2\pi k + \theta_2 \text{ with } k \text{ being an integer,} \\ 0, & \text{otherwise.} \end{cases} \tag{2.13}$$

In [8], Zheng et al. used Eqn. 2.11 to give an analytical force model in angular domain using Fourier series expansion. For the derivation of the analytical model, two coordinate systems are utilized. The rectangular $X - Y - Z$ coordinate system is used for force expressions and $R - \phi - Z$ cylindrical coordinate system for the rotating cutter as seen in Fig. 2.1.

The explicit functions in Eqn. 2.11 should be rewritten in Fourier series expansion. To start with, the windowing function can be expressed as the following equation in Fourier series.

$$w(\theta) = \frac{a_0}{2} + \sum_{k=1}^{\infty} a_k \cos k\theta + \sum_{k=1}^{\infty} b_k \sin k\theta, \tag{2.14}$$

where

$$a_0 = \frac{\theta_2 - \theta_1}{\pi}, \quad a_k = \frac{\sin k\theta_2 - \sin k\theta_1}{k\pi}, \quad b_k = \frac{\cos k\theta_1 - \cos k\theta_2}{k\pi} \tag{2.15}$$

To include the axial engagement for each of the cutting flute, the spindle position should be converted into cutter position.

$$\theta = \phi - \beta \tag{2.16}$$

Combining Eqn. 2.14 and 2.16 to the general force expression Eqn. 2.11 one can get the force expression.

$$\begin{bmatrix} f_x(\phi) \\ f_y(\phi) \\ f_z(\phi) \end{bmatrix} = k_t \cdot K \cdot t_x \cdot b_h \int_0^{\beta_0} \sum_{m=0}^{N-1} \begin{bmatrix} p_1\left(\phi - \beta - \frac{2m\pi}{N}\right) \\ p_2\left(\phi - \beta - \frac{2m\pi}{N}\right) \\ p_3\left(\phi - \beta - \frac{2m\pi}{N}\right) \end{bmatrix} \times \left\{ \frac{a_0}{2} + \sum_{k=1}^{\infty} a_k \cdot \cos k\left(\phi - \beta - \frac{2k\pi}{N}\right) + \sum_{k=1}^{\infty} b_k \cdot \sin k\left(\phi - \beta - \frac{2k\pi}{N}\right) \right\} d\beta. \tag{2.17}$$

Using the equations of:

$$\sum_{k=0}^{N-1} \sin\left(\theta + \frac{2k\pi}{N}\right) = \begin{cases} N \sin\theta, & \text{if } k \text{ is harmonics of } N, \\ 0, & \text{otherwise} \end{cases} \tag{2.18}$$

$$\sum_{k=0}^{N-1} \cos\left(\theta + \frac{2k\pi}{N}\right) = \begin{cases} N \cos\theta, & \text{if } k \text{ is harmonics of } N, \\ 0, & \text{otherwise} \end{cases} \tag{2.19}$$

the elementary cutting function $p_1(\theta)$ can be written as:

$$\sum_{k=0}^{\infty} p_1(\phi - \beta - \frac{2m\pi}{N}) = N \cdot p_1(\phi - \beta) = N \cdot \frac{sin(2\theta)}{2} \tag{2.20}$$

Using the coefficients as:

$$a_{n0} = \frac{1}{\pi}\int_{\theta_1}^{\theta_2} f(\theta)\, d\theta, a_n = \frac{1}{\pi}\int_{\theta_1}^{\theta_2} f(\theta) \cdot \cos(n\theta)\, d\theta \quad b_n = \frac{1}{\pi}\int_{\theta_1}^{\theta_2} f(\theta) \cdot \sin(n\theta)\, d\theta \tag{2.21}$$

the Fourier series coefficients for $p_1(\theta)$ can be written using Eqn. 2.20 such that:

$$a_{n0} = \frac{1}{\pi}\int_{\theta_1}^{\theta_2} f(\theta)\, d\theta = \frac{1}{\pi}\int_{\theta_1}^{\theta_2} N \cdot \frac{sin(2\theta)}{2}\, d\theta = \frac{N}{2\pi}\frac{cos(2\theta_1) - cos(2\theta_2)}{2} = \frac{N}{2} \cdot b_2 \tag{2.22}$$

where b_2 is the equation of b_k with $k = 2$ in Eqn. 2.15. Multiplying a_{n0} with $\frac{a_0}{2}$ of the window function where $\theta_1 = 0$ and $\theta_2 = \beta_0$ from the integration of Eqn. 2.17, DC component of the first elementary cutting function is expressed as:

$$A_0^{p_1} = a_{n0} \cdot a_0 = \frac{N}{2} \cdot b_2 \cdot \frac{\beta_0}{2} = \frac{b_2}{4} \cdot N\beta_0 \tag{2.23}$$

For coefficient a_n:

$$a_n = \frac{1}{\pi}\int_{\theta_1}^{\theta_2} f(\theta) \cdot \cos(n\theta)\, d\theta = \frac{1}{\pi}\int_{\theta_1}^{\theta_2} \frac{sin(2\theta)}{2} \cdot \cos(n\theta)\, d\theta \tag{2.24}$$

Using the Product-to-Sum conversion of sine and cosine;

$$a_n = \frac{1}{2\pi}\int_{\theta_1}^{\theta_2} sin(2\theta)\cdot\cos(n\theta)\,d\theta = \frac{1}{2\pi\cdot 2}\int_{\theta_1}^{\theta_2}[sin(2\theta+n\theta)+\sin(2\theta-n\theta)]\,d\theta$$

$$= \frac{1}{2\pi\cdot 2}\int_{\theta_1}^{\theta_2}(sin[(n+2)\theta]+\sin[(n-2)\theta])\,d\theta$$

$$= \frac{-1}{2\pi\cdot 2}\cdot\left[\frac{cos[(n+2)\theta]}{n+2}+\frac{cos[(n-2)\theta]}{n-2}\right]_{\theta_1}^{\theta_2}$$

$$A_k^{p_1} = \frac{b_{k+2}-b_{k-2}}{2k} \tag{2.25}$$

where Eqn. 2.25 is the equation of b_k with $n = k+2$ and $n = k-2$ in Eqn. 2.15. Integrating the harmonic multiplicator cosine of the coefficient a_k where $\theta_1 = 0$ and $\theta_2 = \beta_0$ from the integration of Eqn. 2.17, that term becomes:

$$\int_0^{\beta_0} cos[k\cdot(\phi-\beta)]\cdot d\beta = \Big[sin[k\cdot(\phi-\beta)]\Big]_0^{\beta_0} = sin[k\cdot(\phi-\beta_0)]-sin(k\cdot\phi) \tag{2.26}$$

Using the trigonometric addition identities Eqn. 2.26 is rewritten as;

$$\int_0^{\beta_0} cos[k\cdot(\phi-\beta)]\cdot d\beta = 2\cdot cos[k\cdot(\phi-\frac{\beta_0}{2})]\cdot sin(-\frac{k\cdot\beta_0}{2}) \tag{2.27}$$

For coefficient b_n:

$$b_n = \frac{1}{\pi}\int_{\theta_1}^{\theta_2} f(\theta)\cdot\sin(n\theta)\,d\theta = \frac{1}{\pi}\int_{\theta_1}^{\theta_2}\frac{sin(2\theta)}{2}\cdot\sin(n\theta)\,d\theta \tag{2.28}$$

Using the Product-to-Sum conversion of sine and cosine;

$$b_n = \frac{1}{2\pi}\int_{\theta_1}^{\theta_2} sin(2\theta)\cdot\sin(n\theta)\,d\theta = \frac{1}{2\pi\cdot 2}\int_{\theta_1}^{\theta_2}[cos(2\theta-n\theta)-\cos(2\theta+n\theta)]\,d\theta$$

$$= \frac{1}{2\pi\cdot 2}\int_{\theta_1}^{\theta_2}(-cos[(n-2)\theta]-\cos[(n+2)\theta])\,d\theta$$

$$= \frac{-1}{2\pi\cdot 2}\cdot\left[\frac{sin[(n-2)\theta]}{n-2}+\frac{sin[(n+2)\theta]}{n+2}\right]_{\theta_1}^{\theta_2}$$

$$B_k^{p_1} = \frac{a_{k-2}-a_{k+2}}{2k} \tag{2.29}$$

where Eqn. 2.29 is the equation of b_k with $n = k+2$ and $n = k-2$ in Eqn. 2.15. Integrating the harmonic multiplicator sine of the coefficient b_k where $\theta_1 = 0$ and $\theta_2 = \beta_0$ from the integration of Eqn. 2.17, that term becomes:

$$\int_0^{\beta_0} sin[k\cdot(\phi-\beta)]\cdot d\beta = \Big[-cos[k\cdot(\phi-\beta)]\Big]_0^{\beta_0} = -cos[k\cdot(\phi-\beta_0)]+cos(k\cdot\phi) \tag{2.30}$$

Using the trigonometric addition identities Eqn. 2.30 is rewritten as;

$$\int_0^{\beta_0} sin[k\cdot(\phi-\beta)]\cdot d\beta = 2\cdot sin[k\cdot(\phi-\frac{\beta_0}{2})]\cdot sin(\frac{k\cdot\beta_0}{2}) \tag{2.31}$$

The components in Equations 2.23, 2.25, 2.27, 2.29, 2.31 are derived for the first elementary cutting function $p_1(\theta)$. It is already known that the cutting functions have a value for the harmonics of tooth number. Otherwise they become zero. Therefore, the term k is replaced with $k\cdot N$. With the same calculation process, the angular domain Fourier series expansions can be obtained for $p_2(\theta)$ and $p_3(\theta)$. Finally, substituting them all into the Equation 2.17, the angular domain force expression can be expressed as the following equation with q number of harmonics as in [8].

$$\begin{aligned}\begin{bmatrix} f_x(\phi) \\ f_y(\phi) \\ f_z(\phi) \end{bmatrix} &= k_t\cdot K\cdot t_x\cdot b_h \begin{bmatrix} \frac{b_2}{4} \\ \frac{a_0-a_2}{4} \\ \frac{b_1}{2} \end{bmatrix} N\beta_0 \\ &+\sum_{k=1}^{q}\sin\left(\frac{kN\beta_0}{2}\right)\left(\begin{bmatrix} \frac{a_{kN-2}-a_{kN+2}}{2k} \\ \frac{2b_{kN}-b_{kN-2}-b_{kN+2}}{2k} \\ \frac{a_{kN-1}-a_{kN+1}}{k} \end{bmatrix}\times\sin\left(kN\left(\phi-\frac{\beta_0}{2}\right)\right)\right. \\ &\left.+\begin{bmatrix} \frac{b_{kN+2}-b_{kN-2}}{2k} \\ \frac{2a_{kN}-a_{kN-2}-a_{kN+2}}{2k} \\ \frac{b_{kN+1}-b_{kN-1}}{k} \end{bmatrix}\times\cos\left(kN\left(\phi-\frac{\beta_0}{2}\right)\right)\right)\end{aligned} \tag{2.32}$$

The Eqn. 2.32 gives the x, y and z components of the cutting force, with empirically determined k_t coefficient and K ratio matrix through angular convolution modelling. The net force consists of the sum of pre-determined number of harmonics. The inputs of the force model in addition to cutting coefficients are the tool geometry and process parameters such as depths of cut, entrance and exit angles.

The force expression derived in Eqn. 2.32 is providing to calculate the forces with two cutting coefficients. In [7] and [29-31], it is mentioned that edge coefficients play an important role in the modeling of milling forces. They ensure that the effects of the tool's edge geometry and its engagement with the workpiece are included in the calculations. The edge coefficients are describing the edge and friction characteristics of the tool and provide more accurate cutting force values. Therefore, in this thesis, it

is decided to work with two cutting and two edge coefficients. As discussed before, Eqn. 2.32 calculates the force with two cutting coefficients in angular domain. In [7], Wang and Zheng rewrites the Eqn. 2.3 by adding the edge coefficients.

$$f_t(\theta) = k_t \cdot t_x \cdot sin\theta + k_{te} \quad \text{and} \quad f_r(\theta) = k_t \cdot k_r \cdot t_x \cdot sin\theta + k_{te} \cdot k_{re} \tag{2.33}$$

The elementary cutting coefficients in Eqn. 2.7 is rewritten for x and y coordinates by adding the edge coefficients as follows:

$$\begin{pmatrix} p_x(\theta) \\ p_y(\theta) \end{pmatrix} = t_x \cdot \begin{pmatrix} 1 & k_r \\ -k_r & 1 \end{pmatrix} \begin{pmatrix} p_1(\theta) \\ p_2(\theta) \end{pmatrix} + \begin{pmatrix} 1 & k_{re} \\ -k_{re} & 1 \end{pmatrix} \begin{pmatrix} p_3(\theta) \\ p_4(\theta) \end{pmatrix} \tag{2.34}$$

where

$$p_1(\theta) = \frac{1}{2} \cdot sin(2\theta), \quad p_2(\theta) = \frac{1}{2} \cdot (1 - cos(2\theta)) \tag{2.35}$$

$$p_3(\theta) = cos(\theta), \quad p_4(\theta) = sin(\theta) \tag{2.36}$$

In this thesis, as a novelty, the elementary cutting functions for edge coefficients $p_3(\theta)$ and $p_4(\theta)$ are added into the angular domain convolution force model. Since the concern of the work is x and y force, the expression of z force is neglected for simplicity.

$$\begin{aligned} \begin{bmatrix} f_x(\phi) \\ f_y(\phi) \end{bmatrix} &= k_t \cdot K \cdot t_x \cdot b_h \begin{bmatrix} \frac{b_2}{4} \\ \frac{a_0 - a_2}{4} \end{bmatrix} N\beta_0 \\ &+ \sum_{k=1}^{q} \sin\left(\frac{kN\beta_0}{2}\right) \left(\begin{bmatrix} \frac{a_{kN-2} - a_{kN+2}}{2k} \\ \frac{2b_{kN} - b_{kN-2} - b_{kN+2}}{2k} \end{bmatrix} \times \sin\left(kN\left(\phi - \frac{\beta_0}{2}\right)\right) \right. \\ &+ \left. \begin{bmatrix} \frac{b_{kN+2} - b_{kN-2}}{2k} \\ \frac{2a_{kN} - a_{kN-2} - a_{kN+2}}{2k} \end{bmatrix} \times \cos\left(kN\left(\phi - \frac{\beta_0}{2}\right)\right) \right) \end{aligned} \tag{2.37}$$

As mentioned in [7], the edge parameters are independent of chip thickness which cancels the multiplication of those terms with feed rate, t_x. Therefore, t_x term is moved into the cutting coefficients terms which are first two rows of the matrices. The Equation 2.37 is rewritten by adding elementary cutting functions of edge coefficients, multiplying feed rate with only cutting coefficient terms, combining k_t coefficient and K matrix in K_4 matrix for coefficient simplicity. The elementary cutting functions for edge coefficients given in Equation 2.36, have to be converted

into Fourier series form in order to be combined to the force expression derived in Equation 2.37. Following the Equations from 2.21 to 2.30, the elementary cutting functions for edge coefficients can be transformed into Fourier harmonics and at the end, the force can be expressed with two edge and two cutting coefficients as:

$$\begin{bmatrix} f_x(\phi) \\ f_y(\phi) \end{bmatrix} = K_4 \cdot b_h \begin{bmatrix} \frac{t_x \cdot b_2}{4} \\ \frac{t_x \cdot (a_0 - a_2)}{4} \\ \frac{a_1}{2} \\ \frac{b_1}{2} \end{bmatrix} N\beta_0 + \sum_{k=1}^{q} \sin\left(\frac{kN\beta_0}{2}\right) \left(\begin{bmatrix} \frac{t_x \cdot (a_{kN-2} - a_{kN+2})}{2k}) \\ \frac{t_x \cdot (2b_{kN} - b_{kN-2} - b_{kN+2})}{2k} \\ \frac{b_{kN-1} + b_{kN+1}}{k} \\ \frac{a_{kN-1} - a_{kN+1}}{k} \end{bmatrix} \times \sin\left(kN\left(\phi - \frac{\beta_0}{2}\right)\right) + \begin{bmatrix} \frac{t_x \cdot (b_{kN+2} - b_{kN-2})}{2k} \\ \frac{t_x \cdot (2a_{kN} - a_{kN-2} - a_{kN+2})}{2k} \\ \frac{a_{kN+1} + a_{kN-1}}{k} \\ \frac{b_{kN+1} - b_{kN-1}}{k} \end{bmatrix} \times \cos\left(kN\left(\phi - \frac{\beta_0}{2}\right)\right) \right) \tag{2.38}$$

where the coefficient matrix is:

$$K_4 = \begin{bmatrix} K_t & K_r & K_{te} & K_{re} \\ -K_r & K_t & -K_{re} & K_{te} \end{bmatrix}$$

In order to validate the necessity of additional two edge coefficients, a real cutting test with pre-known coefficients is conducted. The coefficients was found with average force method explained in [29] and given in Table 2.1. The process parameters are as in Table 2.2. The cutting forces from Eqn.2.37 and Eqn.2.38 are calculated using those parameters and compared in Figure 2.2 with real test force collected from dynamometer.

Table 2.1: Cutting and Edge Parameters for Cutting Test

Parameter	**Symbol**	**Value**	**Unit**
Tangential Cutting Coefficient	K_t	272.6	$\mathrm{N/mm^2}$
Radial Cutting Coefficient	K_r	23.09	$\mathrm{N/mm^2}$
Tangential Edge Coefficient	K_{te}	44.06	$\mathrm{N/mm}$
Radial Edge Coefficient	K_{re}	28.4	$\mathrm{N/mm}$

Table 2.2: Process Parameters for Cutting Test

Parameter	**Symbol**	**Value**	**Unit**
Spindle Speed	$\dot{\Phi}$	4500	rpm
Feed Speed	t_x	0.1111	mm/tooth
Cutter Diameter	D	12	mm
Tooth Number	N	3	-
Helix Angle	α	45	deg
Depth of Cut	a_p	2	mm
Radial Depth of Cut	a_e	6	mm

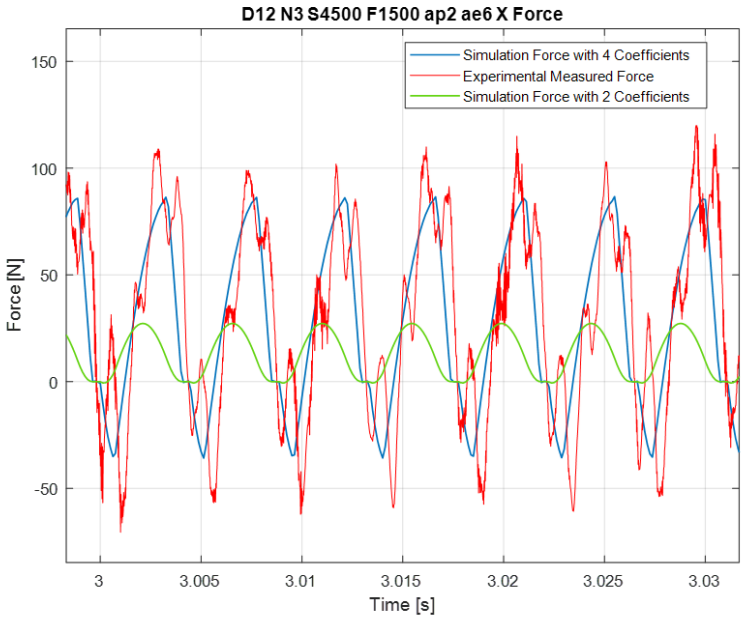

Figure 2.2: Force Comparison

The two cutting coefficient model is oscillating between 30 N and 0 N. As seen from the difference of forces, it can be said that the dominant part of the cutting force for this cutting case consists of the edge parameters. Adding the two edge coefficients to the force model affected the force to oscillate between 80 N and -30 N as seen in Figure 2.2. With the increasing number of harmonics, the simulation values can be closer to the real experimental values. The calculation of cutting force including the edge coefficients gives more accurate results as shown in Figure 2.2.

CHAPTER 3

MILLING FORCE ESTIMATION MODEL

3.1 Milling Dynamics

After the mechanical interaction between tool and workpiece becomes steady, the force starts to oscillate periodically for constant process parameters. This force causes the workpiece to vibrate depending on its dynamic response characteristics which is the Frequency Response Function. The FRF of the workpiece can be obtained with a modal test.

The Frequency Response Function, FRF, is the characteristics of a system to a known input. The input can be provided with an impact hammer or with a modal shaker and the response is measured with a sensor. The sensor can be chosen according to the type of the FRF. It can be accelerometer for accelerance which is acceleration per unit force, velocity probe for mobility which is velocity per unit force or a displacement sensor for receptance which is displacement per unit force. Accelerance and receptance are the most common values to calculate frequency response functions. In this study, accelerance is used to identify the workpiece.

In milling, the known input is the cutting force and the response is the acceleration. The dynamic characteristics of the workpiece can be found and represented as a transfer function. The acceleration due to cutting forces occurs according to the accelerance of the workpiece. Mathematically, the cutting force multiplied with accelerance gives the acceleration. Multiplication operation can be done in Laplace domain as follows:

$$Y(s) = G(s) \cdot X(s)$$

where $Y(s)$ is the output, $G(s)$ is the transfer function and $X(s)$ is the input. Rewrit-

ing the multiplication according to milling cutting:

$$A(s) = G_{acc}(s) \cdot F(s) \tag{3.1}$$

where $A(s)$ is the acceleration, $G_{acc}(s)$ is the accelerance of workpiece and $F(s)$ is the cutting force.

In addition to Eqn. 3.1, the harmonics of force and acceleration can be related with each other at specific frequencies using FRF. In other words, for a specific frequency, the relation between acceleration and the force is a gain which can be taken from FRF of the workpiece. It is valid for each frequency and can be expressed as:

$$|A(f_1)| = |G_{acc}(f_1)| \cdot |F(f_1)|$$

$$|A(f_2)| = |G_{acc}(f_2)| \cdot |F(f_2)|$$

$$...$$

$$|A(f_n)| = |G_{acc}(f_n)| \cdot |F(f_n)|$$

where f_1, f_2 and f_n are the relevant frequencies.

In this study, the force expression developed in Chapter 2 is used. It does not include the run-out of the spindle, therefore the expression consists only the of the harmonics at the orders of tooth passing frequency, which are the multiples of spindle frequency multiplied with tooth number. Using the FRF of workpiece, for each order of tooth passing frequency, the amplitudes of force harmonics found in Eqn. 2.38 are multiplied with the gains of FRF at the related frequencies to find the acceleration. Moreover, the phase delays of FRF should be added to the force harmonics' phase angles to find the phases of acceleration harmonics. Consequently, the acceleration and force relation can be written as:

$$|A(f_n)| = |G(f_n)| \cdot |F(f_n)| \tag{3.2}$$

$$\angle A(f_n) = \angle G(f_n) + \angle F(f_n) \tag{3.3}$$

where $A(f_n)$ is the acceleration harmonics, $F(f_n)$ is the force harmonics from Eqn. 2.38 and $G(f_n)$ is the FRF gains for relevant frequencies. As an example, the gains and the phase angles at the tooth passing frequencies used to convert the force harmonics into the acceleration harmonics are the red marks on the Fig. 3.1.

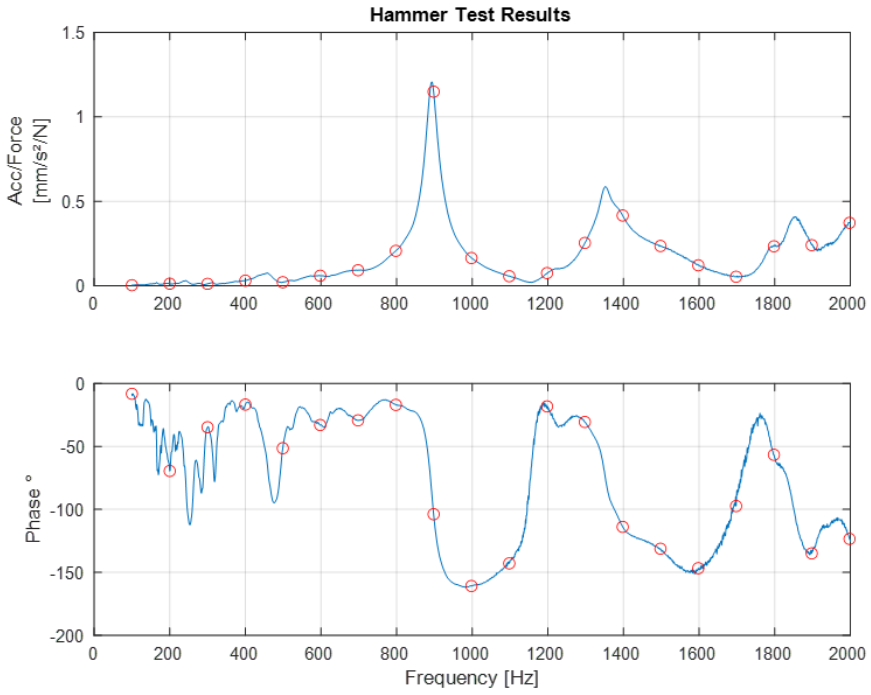

Figure 3.1: Tooth Passing Frequencies Marked on the FRF Results

Following the Equations 3.2 and 3.3, the acceleration which is derived using force equation 2.38 and FRF can be expressed as:

$$\begin{bmatrix} f_x(\phi) \\ f_y(\phi) \end{bmatrix} = K_4 \cdot b_h \begin{bmatrix} \frac{t_x \cdot b_2}{4} \\ \frac{t_x \cdot (a_0 - a_2)}{4} \\ \frac{a_1}{2} \\ \frac{b_1}{2} \end{bmatrix} N\beta_0 + \sum_{k=1}^{q} \sin\left(\frac{kN\beta_0}{2}\right) \left(\begin{bmatrix} \frac{t_x \cdot (a_{kN-2} - a_{kN+2})}{2k}) \\ \frac{t_x \cdot (2b_{kN} - b_{kN-2} - b_{kN+2})}{2k} \\ \frac{b_{kN-1} + b_{kN+1}}{k} \\ \frac{a_{kN-1} - a_{kN+1}}{k} \end{bmatrix} \times \sin\left(kN\left(\phi - \frac{\beta_0}{2}\right)\right) + \begin{bmatrix} \frac{t_x \cdot (b_{kN+2} - b_{kN-2})}{2k} \\ \frac{t_x \cdot (2a_{kN} - a_{kN-2} - a_{kN+2})}{2k} \\ \frac{a_{kN+1} + a_{kN-1}}{k} \\ \frac{b_{kN+1} - b_{kN-1}}{k} \end{bmatrix} \times \cos\left(kN\left(\phi - \frac{\beta_0}{2}\right)\right) \right) \tag{3.4}$$

$$\begin{bmatrix} a_x(\phi) \\ a_y(\phi) \end{bmatrix} = K_4 \cdot b_h \Bigg\{ \sum_{k=1}^{q} |G(f_k)| \cdot \sin\left(\frac{kN\beta_0}{2}\right) \Bigg\{ \begin{bmatrix} \frac{t_x \cdot (a_{kN-2} - a_{kN+2})}{2k} \\ \frac{t_x \cdot (2b_{kN} - b_{kN-2} - b_{kN+2})}{2k} \\ \frac{b_{kN-1} + b_{kN+1}}{k} \\ \frac{a_{kN-1} - a_{kN+1}}{k} \end{bmatrix} \times \sin\left(\angle G(f_k) + kN\left(\phi - \frac{\beta_0}{2}\right)\right) + \begin{bmatrix} \frac{t_x \cdot (b_{kN+2} - b_{kN-2})}{2k} \\ \frac{t_x \cdot (2a_{kN} - a_{kN-2} - a_{kN+2})}{2k} \\ \frac{a_{kN+1} + a_{kN-1}}{k} \\ \frac{b_{kN+1} - b_{kN-1}}{k} \end{bmatrix} \times \cos\left(\angle G(f_k) + kN\left(\phi - \frac{\beta_0}{2}\right)\right) \Bigg\} \Bigg\} \tag{3.5}$$

3.2 System Model

In the previous chapters, the force expression is given as explicit functions of cutting process. After, in case of having FRF of the workpiece, it is clearly explained that how the acceleration expression is derived. Consequently, the acceleration is expressed as a function of some measure, known and unknown parameters.

$$Acceleration = f(\underbrace{\phi_s, t_x}_{\textbf{Measured}}, \underbrace{\phi_{st}, \phi_{ex}, a_p, a_e, FRF}_{\textbf{KnownPreviously}}, \underbrace{K_t, K_r, K_{te}, K_{re}}_{\textbf{Unknown}})$$

In the estimation part of the thesis, the Kalman filter will try to predict the cutting force by iteratively solving the cutting coefficients. The state matrix of the system consist of the cutting coefficients which are two shear and two edge coefficients.

$$\mathbf{x} = \begin{bmatrix} K_t & K_r & K_{te} & K_{re} \end{bmatrix}^T$$

The states are assumed to be not changing with time, in other words, the coefficients are not changing with time.

$$\dot{x} = 0 \quad \text{or in discrete form} \quad q_{k+1} = I \cdot q_k$$

If noise exists in system model:

$$q_{k+1} = \Phi \cdot q_k + w_k \tag{3.6}$$

The state equations can be written as following:

$$\mathbf{\Phi} = \begin{pmatrix} 1 & 0 & 0 & 0 \\ 0 & 1 & 0 & 0 \\ 0 & 0 & 1 & 0 \\ 0 & 0 & 0 & 1 \end{pmatrix}, \quad \mathbf{q} = \begin{pmatrix} K_t \\ K_r \\ K_{te} \\ K_{re} \end{pmatrix} \tag{3.7}$$

$$\mathbf{q}_{k+1} = \mathbf{\Phi}\mathbf{q}_k, \quad \dot{\mathbf{q}} = 0 \tag{3.8}$$

The measurement data is acceleration. All the acceleration calculations are included in the measurement update equation. Measurement matrix (H) is relating the states which are the coefficients with the measured acceleration. It includes the force model, FRF gains and phases. Measurement matrix (H) can be expressed as follows by rearranging Eqn. 3.5:

$$\underbrace{\begin{pmatrix} a_x(\phi) \\ a_y(\phi) \end{pmatrix}}_{\mathbf{Acc}} = \underbrace{b_h \begin{bmatrix} t_x H_1 & t_x H_2 & H_3 & H_4 \\ -t_x H_2 & t_x H_1 & -H_4 & H_3 \end{bmatrix}}_{\mathbf{H}} \underbrace{\begin{bmatrix} K_t \\ K_r \\ K_{te} \\ K_{re} \end{bmatrix}}_{\mathbf{q}} \tag{3.9}$$

where:

$$H_1 = \sum_{k=1}^{q} |G(f_k)| \sin\left(\frac{kN\beta_0}{2}\right) \times \left[\left(\frac{a_{kN-2} - a_{kN+2}}{2k}\right) \cdot \sin\left(\angle G(f_k) + kN\left(\phi - \frac{\beta_0}{2}\right)\right) + \left(\frac{b_{kN+2} - b_{kN-2}}{2k}\right) \cdot \cos\left(\angle G(f_k) + kN\left(\phi - \frac{\beta_0}{2}\right)\right) \right]$$

$$H_2 = \sum_{k=1}^{q} |G(f_k)| \sin\left(\frac{kN\beta_0}{2}\right) \times \left[\left(\frac{2b_{kN} - b_{kN-2} - b_{kN+2}}{2k}\right) \cdot \sin\left(\angle G(f_k) + kN\left(\phi - \frac{\beta_0}{2}\right)\right) + \left(\frac{2a_{kN} - a_{kN-2} - a_{kN+2}}{2k}\right) \cdot \cos\left(\angle G(f_k) + kN\left(\phi - \frac{\beta_0}{2}\right)\right) \right]$$

$$H_3 = \sum_{k=1}^{q} |G(f_k)| \sin\left(\frac{kN\beta_0}{2}\right) \times \left[\left(\frac{b_{kN-1} + b_{kN+1}}{k}\right) \cdot \sin\left(\angle G(f_k) + kN\left(\phi - \frac{\beta_0}{2}\right)\right) + \left(\frac{a_{kN+1} + a_{kN-1}}{k}\right) \cdot \cos\left(\angle G(f_k) + kN\left(\phi - \frac{\beta_0}{2}\right)\right)\right]$$

$$H_4 = \sum_{k=1}^{q} |G(f_k)| \sin\left(\frac{kN\beta_0}{2}\right) \times \left[\left(\frac{a_{kN-1} - a_{kN+1}}{k}\right) \cdot \sin\left(\angle G(f_k) + kN\left(\phi - \frac{\beta_0}{2}\right)\right) + \left(\frac{b_{kN+1} - b_{kN-1}}{k}\right) \cdot \cos\left(\angle G(f_k) + kN\left(\phi - \frac{\beta_0}{2}\right)\right)\right]$$

3.3 Kalman Structure

Kalman filter is a common way of data fusion, which synthesizes the system's dynamic model with sensor data to find the optimum state values for defined relation of data and mathematical model. As explained in [32], it is an iterative solution to discrete-data filtering. It is used to eliminate the effects of measurement noise and uncertainties of the model. Kalman filter algorithm operates recursively in two phases which are prediction phase and update phase.

In prediction phase, a priory prediction of states (q) and state covariance (P) is done using state transition matrix (Φ), initial or previous estimates (q_0), process noise (w) and process noise covariance (Q).

$$\mathbf{q}_{k+1}^{-} = \mathbf{\Phi} \cdot \mathbf{q}_k \tag{3.10}$$

$$\mathbf{P}_{k+1}^{-} = \mathbf{\Phi} \cdot \mathbf{P}_k \cdot \mathbf{\Phi}^T + \mathbf{Q} \tag{3.11}$$

After, the Kalman gain (K) is calculated using the state covariance (P), measurement matrix (H) which relates the estimated states with measurement data, and measurement noise covariance (R).

$$\mathbf{K}_{k+1} = \mathbf{P}_{k+1}^{-} \cdot \mathbf{H}^T \cdot (\mathbf{H} \cdot \mathbf{P}_{k+1}^{-} \cdot \mathbf{H}^T + \mathbf{R})^{-1} \tag{3.12}$$

In the update phase, the posterior estimate is done for states (q) and state covariance (P) using measurement data z, measurement matrix (H) and Kalman gain (K) in

order to minimize the mean of squared error. Kalman filter balances the prediction and measurement uncertainty and finds the optimum state variables.

$$\mathbf{q}_{k+1} = \mathbf{q}_{k+1}^{-} + \mathbf{K}_{k+1} \cdot (\mathbf{z}_{k+1} - \mathbf{H} \cdot \mathbf{q}_{k+1}^{-}) \tag{3.13}$$

$$\mathbf{P}_{k+1} = (\mathbf{I} - \mathbf{K}_{k+1} \cdot \mathbf{H}) \cdot \mathbf{P}_{k+1}^{-} \tag{3.14}$$

In this study, Kalman filter is used to estimate the cutting forces using acceleration measurement. For a basic Kalman filter structure, the states which are going to be estimated should be separated from the equation set and should be written explicitly. Moreover, since the Kalman filter measurement will be fed with time-series data, the output of system model should also be in time-domain. In other words, measurement matrix (H) and state vector (q) multiplication should give the output directly in time-domain. Since the force calculation methods use the harmonics of the force in the orders of tooth passing frequency, the summation of them should be done before Kalman filter's output calculation as in Eqn. 2.38. That is one of the reasons why that force model is preferred in this thesis.

State matrix (q), state transition matrix (Φ), measurement data z and measurement matrix (H) are given in the previous section. The states (q), are the cutting coefficients. As the output of the Kalman filter, they are estimated depending on the balance between measured and modelled acceleration. After, those coefficients are used to calculate the estimated force using Eqn. 2.38.

3.4 Simulation Model

In order to estimate the cutting forces using acceleration data and FRF of workpiece using Kalman filter, a simulation model is created in MATLAB/Simulink R2020b. To see the effects of workpiece dynamics to the solution, two models are built. In the first model, in order to test the method with basic assumptions a simple second order transfer function is proposed for the workpiece dynamics. In the second model, a more complex workpiece dynamics is constructed. The complexity consists of more than one peak in the bode magnitude plot and sideband frequencies in the results. The transfer functions of the plants are given in Eqns. 3.15 and 3.16.

$$G_1(s) = \frac{0.067s^2}{s^2 + 5.657s + 2e6} \tag{3.15}$$

$$G_2(s) = \frac{2.595e32s^2}{\begin{aligned}(&4e9s^8 + 1.425e13s^7 + 2.639e18s^6 + 6.131e21s^5 + 5.254e26s^4 \\ &+6.766e29s^3 + 3.602e34s^2 + 1.686e37s + 6.919e41)\end{aligned}} \tag{3.16}$$

The bode magnitude plots can be seen in Figure 3.2 and Figure 3.3.

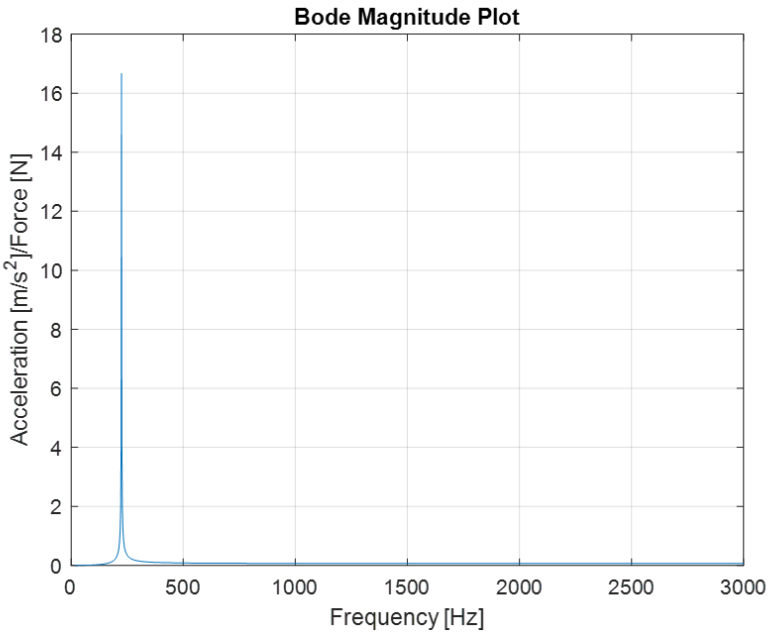

Figure 3.2: First Plant Bode Magnitude Plot

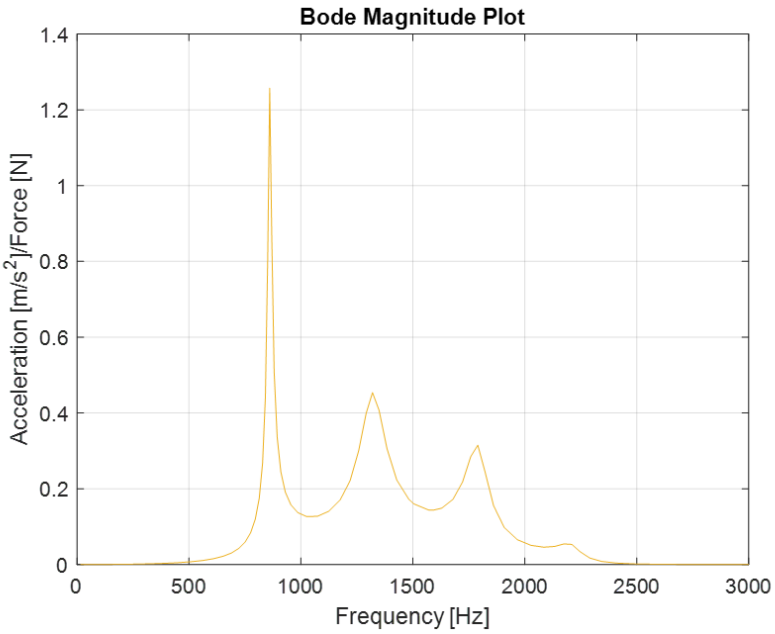

Figure 3.3: Second Plant Bode Magnitude Plot

In Figure 3.4, a schematic representation of numerical simulation is built. The steps for numerical simulation model beginning from force generation to the end force estimation is summarized in that scheme.

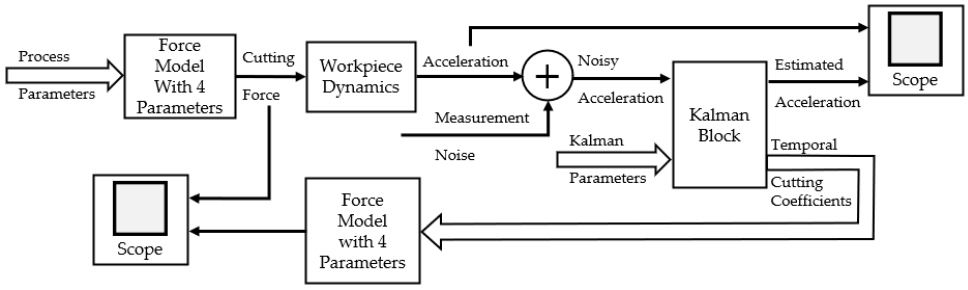

Figure 3.4: Schematic Representation of Numerical Simulation

For the force generation, four parameters force model developed in this work is used with a random set of two cutting, two edge parameters as in Table 3.1 and process parameters as in 3.2. The generated force is seen in Figure 3.5.

Table 3.1: Cutting and Edge Parameters for Simulation Model

Parameter	**Symbol**	**Value**	**Unit**
Tangential Cutting Coefficient	K_t	700	$\mathrm{N/mm^2}$
Radial Cutting Coefficient	K_r	300	$\mathrm{N/mm^2}$
Tangential Edge Coefficient	K_{te}	25	$\mathrm{N/mm}$
Radial Edge Coefficient	K_{re}	35	$\mathrm{N/mm}$

Table 3.2: Process Parameters for Numerical Simulation

Parameter	**Symbol**	**Value**	**Unit**
Spindle Speed	$\dot{\Phi}$	3300	rpm
Feed Speed	t_x	0.1667	mm/tooth
Cutter Diameter	D	12	mm
Tooth Number	N	3	-
Helix Angle	α	45	deg
Depth of Cut	a_p	2	mm
Radial Depth of Cut	a_e	6	mm

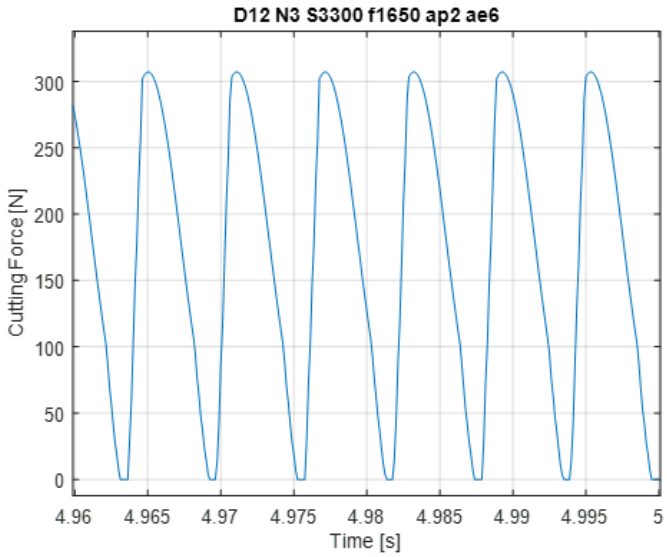

Figure 3.5: Generated Cutting Force for Simulation Model

Using that force and two different workpiece dynamics, the acceleration data is generated for both model. Since the workpiece dynamics are constructed differently, the generated acceleration data is different for each model whereas the exposed force is the same. For the first model acceleration, the workpiece dynamics consists of one natural frequency. The gains in other frequencies are negligible compared to the peak gain. Therefore, the resultant acceleration also contains less number of dominant harmonics and looks more periodic. In the second model acceleration, there exist more than one natural frequencies in workpiece dynamics. The resultant acceleration contains the summation of different dominant harmonics and it makes it harder to dissolve its pattern from the plot. Before running the simulation, a random noise is added to the generated acceleration data. The generated acceleration can be seen in Figure 3.6 and Figure 3.7. The noisy acceleration data is used as the measurement value in Kalman block.

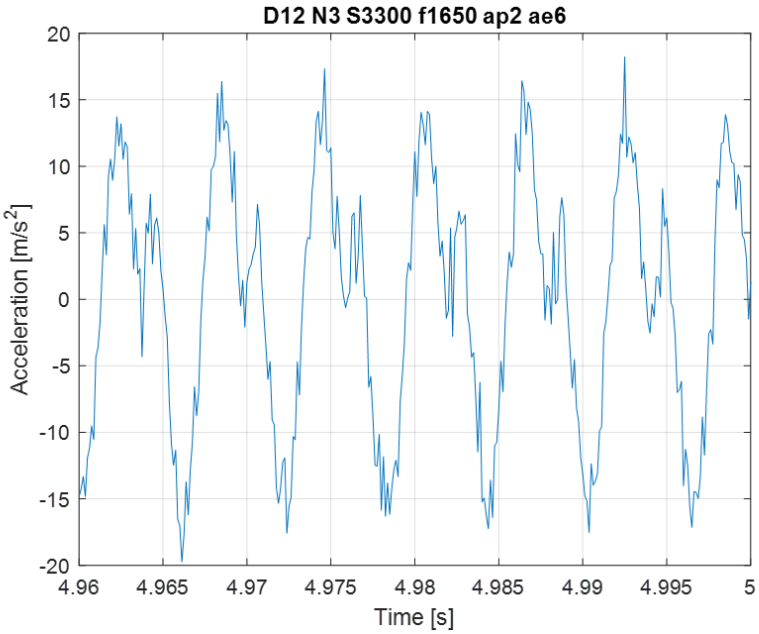

Figure 3.6: First Simulation Plant Model Acceleration Data

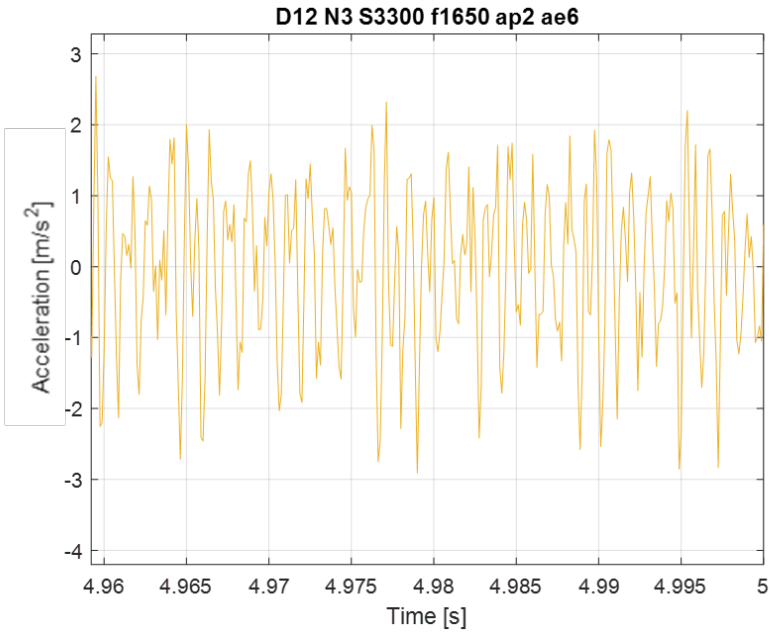

Figure 3.7: Second Simulation Plant Model Acceleration Data

For the Kalman estimation step, initial estimates for states, which are cutting and edge coefficients (q_0), state covariance (P), measurement noise covariance (R) and process noise covariance (Q) are chosen and given as input to Kalman block. The measurement noise covariance is selected according to the random noise added to the generated vibration and process covariance is tuned based on the performance of the Kalman filter. The values are tabulated in Table 3.3. The structure of Kalman Block is seen in Figure 3.8.

Table 3.3: Kalman Variables for Numerical Simulation

Parameter	**Symbol**	**First Model**	**Second Model**
Measurement Covariance	R	4	0.2
Process Covariance	Q	0.5	0.25

3.5 Simulation Results

Kalman block finds the optimum cutting and edge coefficients which balance the measurement acceleration data and calculated acceleration process data depending on the

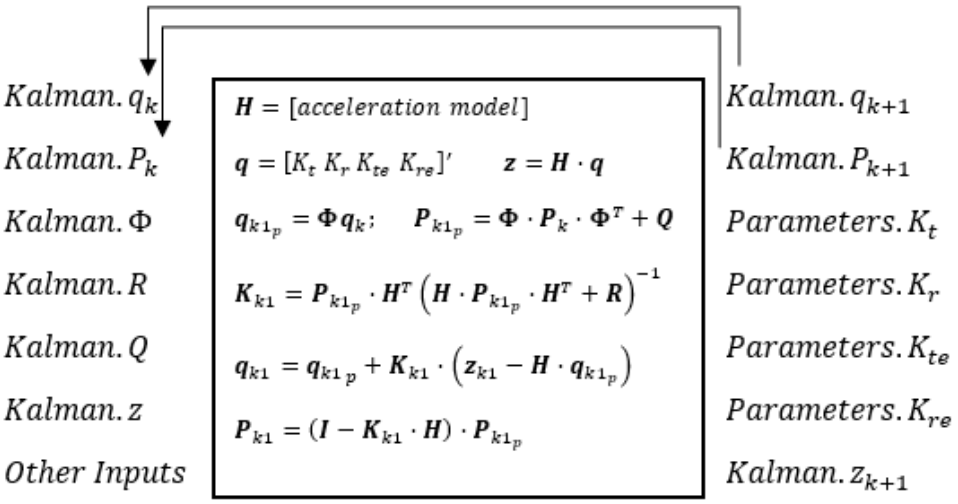

Figure 3.8: Simulink Scheme of Kalman

covariance values. Using those coefficients, the estimated acceleration is calculated as an output of Kalman block and it is compared with measurement acceleration data. In Figure 3.9 and Figure 3.10, it can be seen that Kalman filter estimates the acceleration accurately.

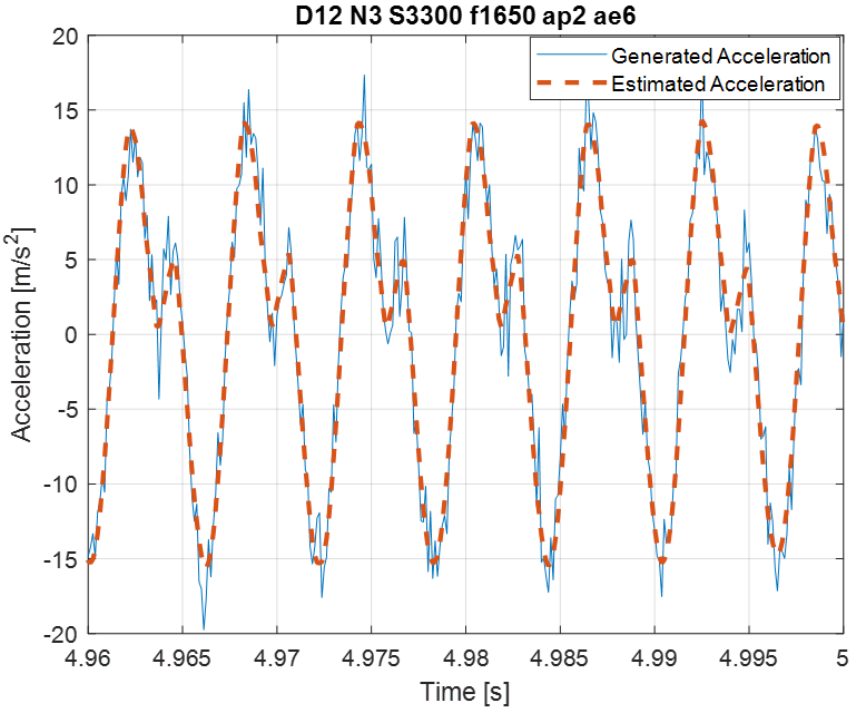

Figure 3.9: First Model Generated and Estimated Acceleration

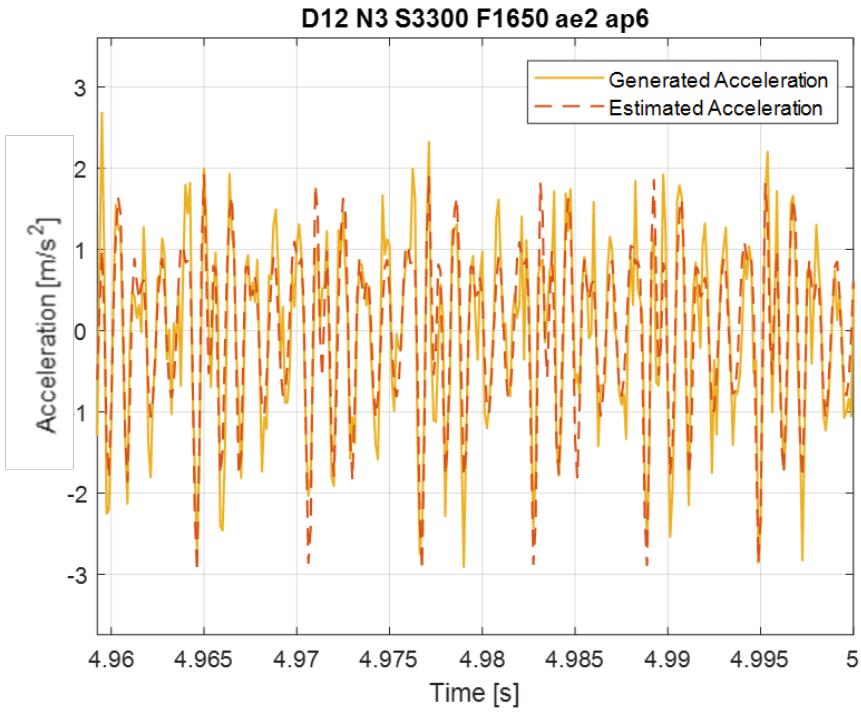

Figure 3.10: Second Model Generated and Estimated Acceleration

When the states which satisfied the accurate acceleration estimates are checked, it is seen in Figure 3.11 that the converged cutting and edge parameters differ from each other in two models. They also differ from generated ones. The reason beyond this is that in practice, same forces can be found with different set of cutting parameters. It depends on the variables of the Kalman parameters. As a result of this, the converged parameters are not expected to be the same in the simulations and tests. Therefore, they can be called temporal parameters.

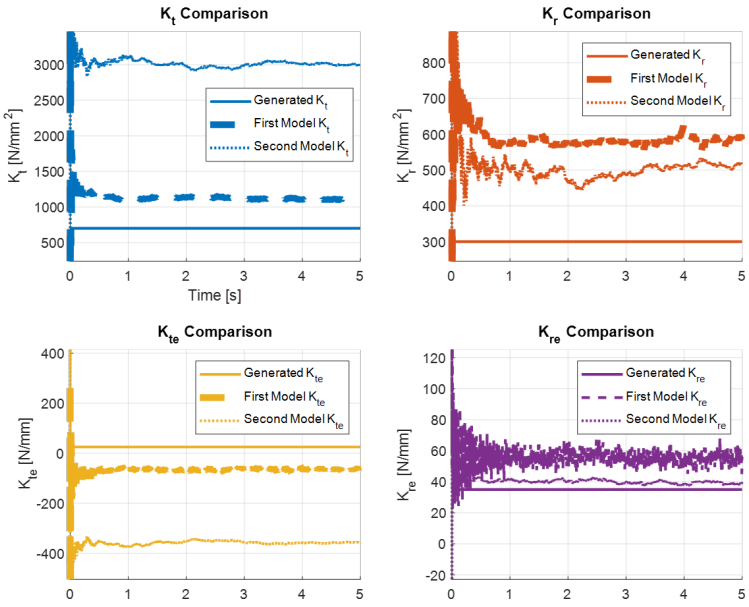

Figure 3.11: Cutting Coefficient Comparison

The important point of the simulation is that the estimated forces should match with each other and the generated force. Using the temporal cutting coefficients, the estimated forces of both model are compared with the generated force in Figure 3.12.

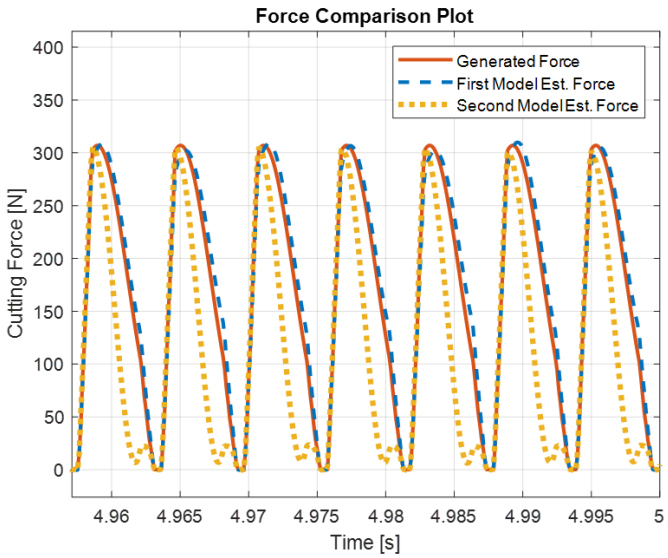

Figure 3.12: Simulation Models Force Comparison

Table 3.4: Results of Simulation Models

Parameter	**Generated Force**	**First Model Estimation**	**Second Model Estimation**
Peak Value	307.07 N	310.03 N	305.71 N
Peak Error	-	1%	1%
RMS	200.05	207.27	157.26
RMS Error	-	4%	21%

In Figure 3.12, it is seen that estimated force from acceleration data for both models and generated force are in similar behaviours. The results are concluded in Table 3.4. The peak values of all forces are very close and the error is less than 1%. When comparing the RMS force values it is seen that the RMS error of first basic model is 4%. The force profiles of first model and generated one are very close because the workpiece has a basic dynamics as mentioned. Acceleration is dominantly related with force harmonics frequencies. Natural frequency of the workpiece does not have a major effect for the first model. The gains in other frequencies are negligible compared to the peak gains. Therefore, it is possible to get a closer force estimation using the resultant acceleration than the second complex dynamics model. In the second model, the workpiece has more than one natural frequencies. The resultant acceleration consists of force harmonics frequencies as the first model and also sideband frequencies of the natural frequencies. The frequency contents of two acceleration data is seen in Figure 3.13.

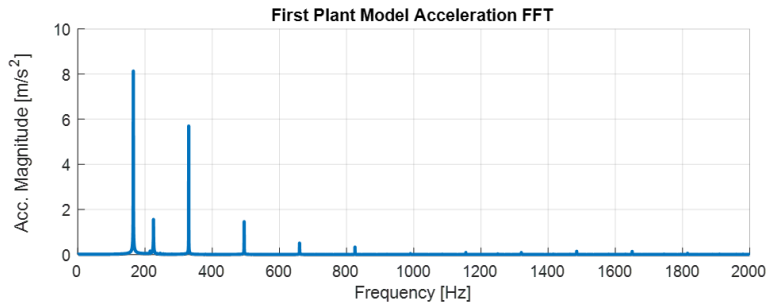

(a) Plant 1

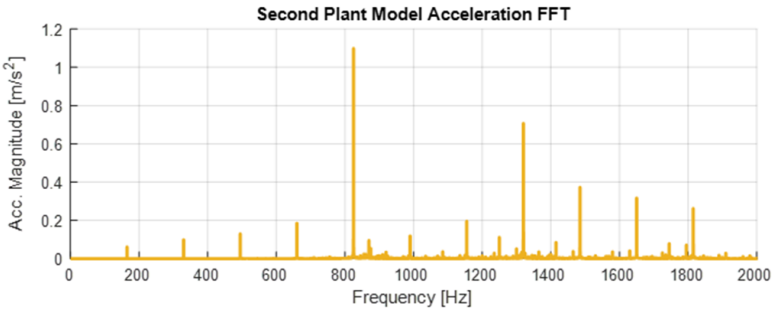

(b) Plant 2

Figure 3.13: Frequency Contents of Two Simulation Acceleration Data

Since the proposed method is using the FRF only in tooth passing frequencies, the harmonics of acceleration in sideband frequencies mislead the Kalman and the estimated force profile diverges from desired value. The estimation algorithm based on the acceleration model derived from force model includes only the harmonics at tooth passing frequencies. The other components are tried to be found also using the tooth passing frequency harmonics which is a misleading way. Therefore, the RMS error of the second plant is about 20% due to the different force profile. To avoid this, in real tests, it is decided to use an acceleration reconstruction algorithm. The measured acceleration will be separated into its frequency components. Starting from the first harmonic to a specific number of harmonics, the acceleration will be recalculated. As a result, despite the complex dynamics, the estimation algorithm was successful in finding the peak values in both plants. In the second plant consisting of complex dynamics, the RMS error was quite higher than expected due to the misleading effects of acceleration. From the results of both models, it is seen that the natural frequencies

and side frequencies affect the Kalman in a wrong way. For more accuracy, the elimination of frequencies other than the tooth passing ones and the structural vibrations should be done before the estimation process. The acceleration data fed to the estimation algorithm will only include the relevant tooth passing frequency components. Combining all the important points from simulation the estimation algorithm can be summarized as in the block diagram given in Figure 3.14.

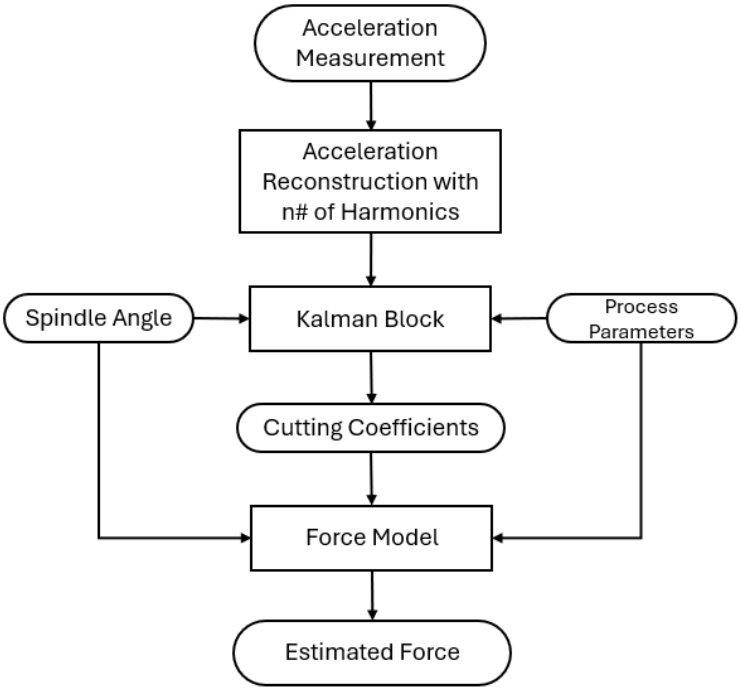

Figure 3.14: Estimation Algorithm Block Diagram

The estimation algorithm starts with the collecting acceleration data. After, to eliminate the structural vibrations and side-frequency components, the acceleration measurement is reconstructed. The measured acceleration data is separated into its harmonics using the FFT algorithm. Next, a number of harmonics of the acceleration FFT is converted into time-domain data with an IFFT algorithm. This operation converts the acceleration data into an equivalent structure with the force model Eqn. 2.34 which forms the basis of the estimation calculations. Reconstructed acceleration data, spindle angle and process parameters are given into the Kalman block. The Kalman block adjusts the state matrix which consists of the cutting coefficients to balance the measurement with the model. Those cutting coefficients are used to make force estimation by using the Eqn. 2.34.

CHAPTER 4

EXPERIMENTAL VERIFICATION

4.1 Test Setup

To support the method and results of simulation model, real cutting tests are done in METU Automatic Control Laboratory. The cutting operation is done on a Deckel FP5CC, 5 axis CNC milling machine which is retrofitted with Beckhoff servo motors, drivers and BECKHOFF C6930 Industrial PC based industrial controller. Hardware and software properties of the test setup is given in the 4.1.

Figure 4.1: Deckel FP5CC CNC Milling Machine

Cutting tests are done with an AL7075 aluminum alloy block. Before the real cutting tests, the spindle run-out is measured via a dial indicator and minimized for a clean cutting test. Otherwise, the method would not work since it does not include the run-out calculations. After, the face which is to be cut is milled for a clean surface. From

Table 4.1: Hardware and Software Properties of the Retrofitted CNC

Unit	**Parameter**	**Description**
CNC Unit	Beckhoff PC	C3690
	TwinCAT-3 Software	Build 4022.29
	ACC Task Sampling Time	125 μs
Spindle	Franz Kessler Motor	10 kW, 9000 rpm
	Beckhoff AX5125 Driver	25 A
	HeidenHain ROD 480 1800	2$''$
X-Y Axes	Beckhoff AM8062 Motor	3000 rpm, 29 Nm
	Beckhoff AX8640 Driver	40 A
	Heidenhain LS 403-0870	1 μm

the clean surface, the axial and radial depths of cut can be set sensitively. All the tests are done with same test setup. The equipments and their specifications are given in the Table 4.2.

Table 4.2: Equipment List and Properties

Equipment	**Model**	**Sensitivity**	**Bandwidth**
Workpiece	Aluminum 7075	N/A	N/A
Impulse Hammer	PCB 086C01	11.2 mV/N	15 kHz
	PCB 086D20	0.23 mV/N	12 kHz
Accelerometer	Dytran 3049E3	99.44 mV/g	10 kHz
	PCB 352C22	11.11 mV/g	10 kHz
Dynamometer	Kistler 9257B	11.2 mV/N	2.3 kHz
Data Acquisition	NI 9234	N/A	Sampling @12.8 kHz
Data Process	Matlab 2020b	N/A	N/A

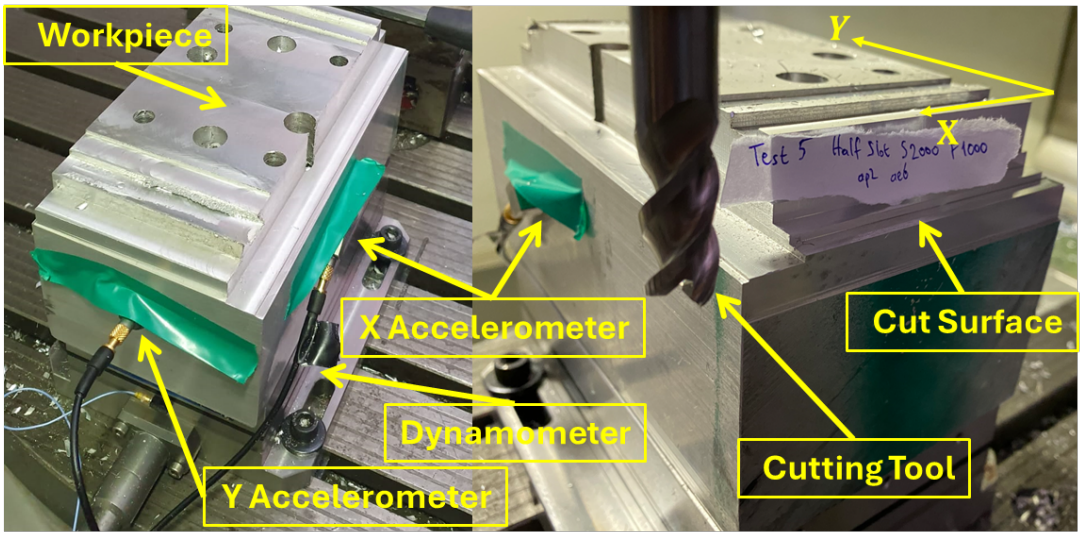

Figure 4.2: Experimental Test Setup

4.2 Frequency Response Function Derivation

Before the cutting test, a modal test is utilized to identify the workpiece dynamics. For the estimation algorithm, the accuracy of FRF is important since it directly affects the relation between force and acceleration. The force is calculated in X and Y directions. To avoid perturbing the different modes of the workpiece during a cutting operation when the cutter moves, the more stable direction should be decided. For this purpose, the FRF's in both directions is checked with a dummy cutting test. The real cutting tests would be done in the short edge of the workpiece, along X direction shown in Figure 4.2. Therefore, the dummy cutting test for FRF direction decision is also done along X direction. During the dummy cutting test, the cutting forces in X and Y directions are measured with dynamometer and accelerations in X and Y directions are measured. In Figure 4.3, FFT plots of the whole cut can be seen. However, to see the effect of position of the spindle to the FRF, FFT's of force and acceleration should be related with respect to the spindle position. As the spindle moves along X axis on the workpiece during cutting, periodically in each 1 second, the force FFT and the acceleration FFT is calculated for X and Y directions. From the dynamics of cutting, it is known that the force harmonics occur in the order frequncies of tooth passing. At those frequencies, the amplitude of acceleration FFT is divided by the amplitudes of force FFT to form the Bode gain plot. The Bode gain plots for X and Y direction

is seen in Figure 4.4. In both directions, the gains in resonance frequencies change depending on the spindle position. However, for the other relevant frequencies, the gains are more stable in Y direction. Therefore, the estimation algorithm is decided to be used with Y direction FRF. Tipping direction is chosen as Y direction and in

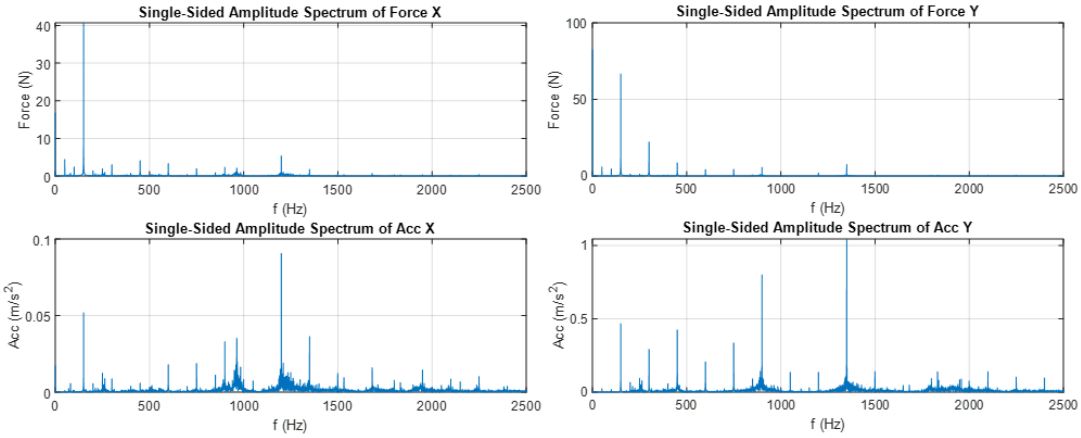

Figure 4.3: X and Y Direction FFT of Force and Acceleration

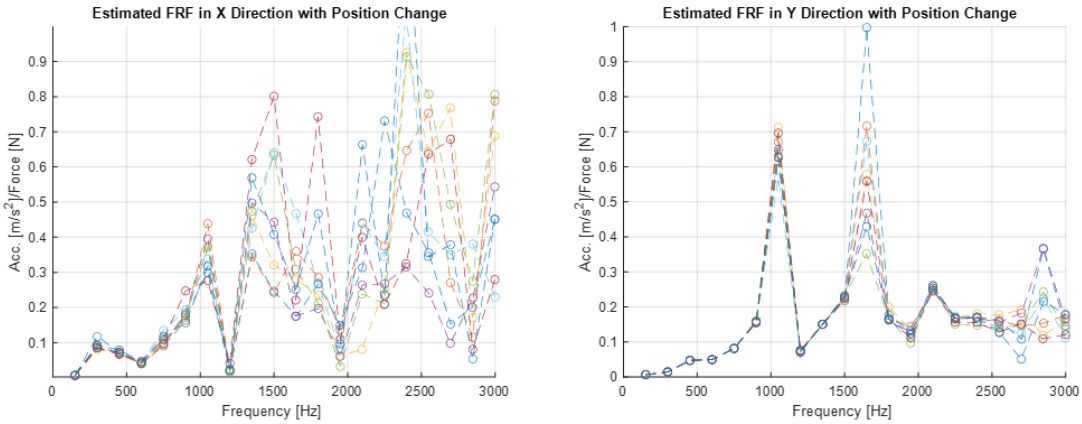

Figure 4.4: X and Y Direction FRF Calculation

the same direction, an accelerometer is attached onto the workpiece as seen in Figure 4.2. The workpiece is tipped in the middle of the short edge and FRF is obtained for Y direction. In Figure 4.6, the FRF of the workpiece in Y direction is plotted. For the estimation algorithm, that FRF is used to relate acceleration and force.

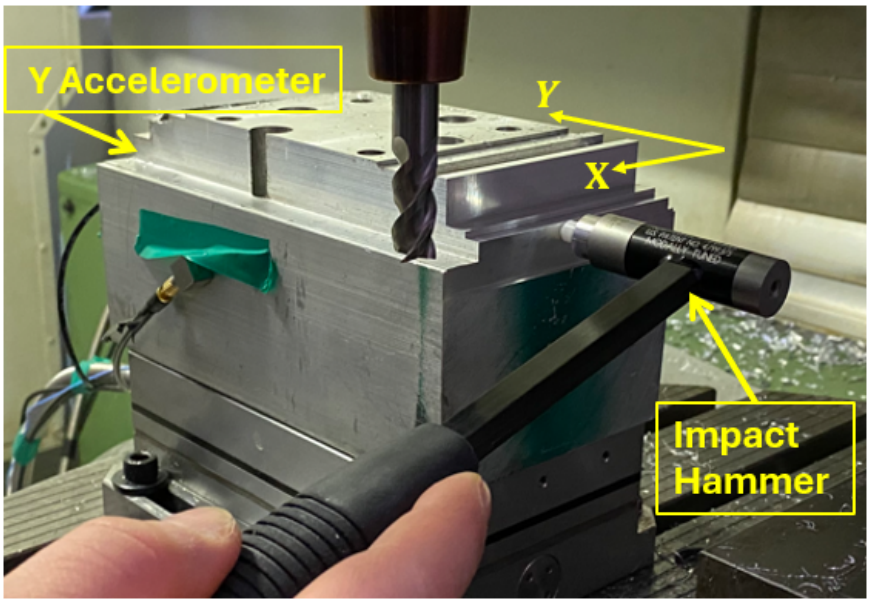

Figure 4.5: Impact Hammer Test

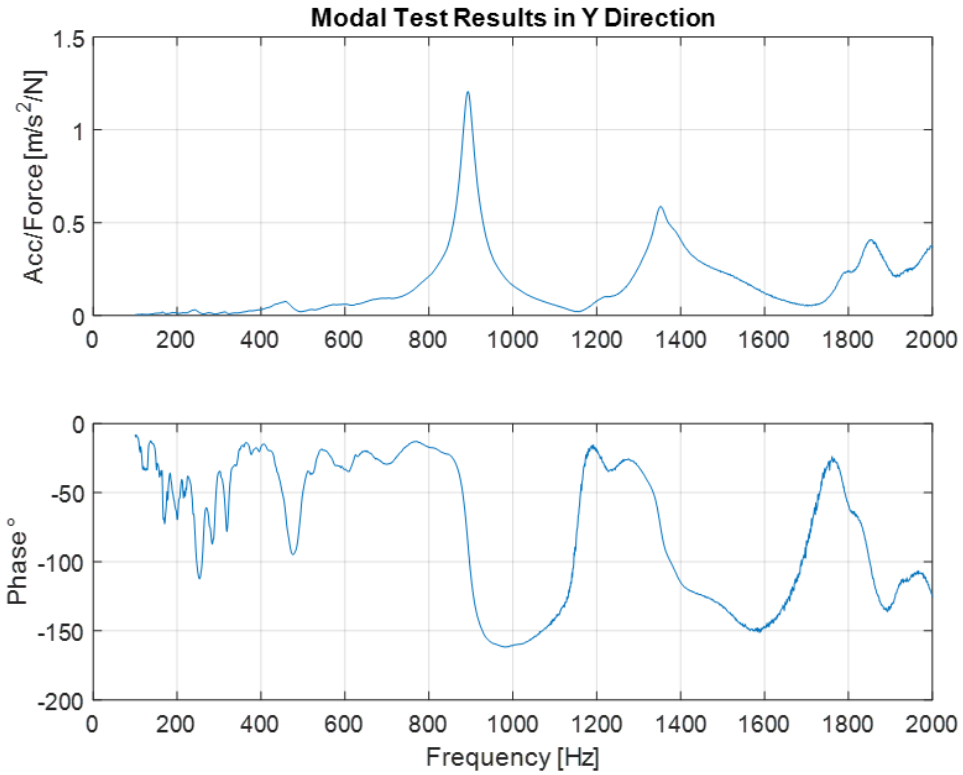

Figure 4.6: Impact Hammer Test Results

4.3 Cutting Tests

To verify the proposed method, real cutting tests are done with different configurations. During cutting, acceleration and force data in Y direction are collected. The acceleration data is processed and an estimation is made for the cutting force. After, the estimated force is compared with the dynamometer force.

In the cutting tests, the following assumptions are made in order to simplify the process.

1. Since the force model Eqn.2.38 is derived for no run-out conditions, it is assumed that no unbalance exists in the spindle. Using a dial indicator the cutter is examined physically. In addition, after each test the FFT of measured force and acceleration is checked. In the existence of a significant run-out, it is expected that some dominant magnitudes are seen in the magnitude plot of FFT at the rotating frequency. For an healthy condition, the dominant magnitudes should be at tooth passing frequencies. With a physical and mathematical confirmation, no run-out is validated for each test.

2. During the cutting process, the spindle moves along the workpiece. When interpreted in terms of FRF inputs and outputs, the input point changes while cutting and mathematically the relation between input and output changes. Although the estimation algorithm is expected and succeed in compensating that change, it should be noted that a constant FRF is used in the calculations.

3. The Kalman filter adjusts the cutting coefficients in order to balance the measured and modeled results of acceleration data. Using the converged coefficients, the force is calculated using Eqn. 2.38. However, the same force can be achieved with different set of cutting parameters. Depending on the cases especially when structural vibrations are dominant, the coefficients may converge to physically meaningless values although the estimated force is in the accepted range. Therefore, the converged coefficients are called the temporal cutting coefficients and the main focus of the work is the estimated force.

4. For adjustment of Kalman covariance values, the measurement covariance is

chosen as the variance of free state acceleration data, without any interference of tool and workpiece. The process covariance is tuned based on the performance of the Kalman filter. For all the tests, the same covariance values are used. They are not controlled for each test.

Table 4.3: Kalman Variables for Estimation Calculations

Parameter	**Symbol**	**Value**
Measurement Covariance	R	0.28
Process Covariance	Q	0.10

5. In the test setup, it is realized that the spindle speed changes very slightly during the cutting operation. It causes shifts in the data which is accumulated in the process of time during cutting. Moreover, it produces numerical deviations. In order to eliminate those effects, the constant spindle speed is fed numerically to the model instead of direct measurement.

6. Lastly, initial spindle angle assumption is needed for the algorithm to converge. The force model, 2.38 is derived in angular domain and strictly depends on the spindle angle. In the test setup, the CNC controlling software and force-acceleration data acquisition systems are not synchronized. The time difference between spindle angle and acceleration must be coherent for the estimation process since the algorithm takes the spindle angle as an input. Initial spindle angle is explained in Subsection 4.3.1.

4.3.1 Initial Spindle Angle Assumption

As mentioned before, the synchronization between spindle angle and acceleration data is vital for the estimation process since the spindle angle is the input of force/acceleration expression. For this purpose, Kline's force model is [5] used as a reference model. With a set of cutting parameters, a simulation is run. The generated force is plotted with the cutter angle in the same plot for three main cases which are half slot up milling, half slot down milling and full slot milling. The purpose of the plot is to

realize the overlapping points of peaks, anti-peaks, zero-crossings etc. of the force and the spindle angle.

1. For half slot up milling it is seen in Figure 4.7 that the peak force is at 90° spindle angle.

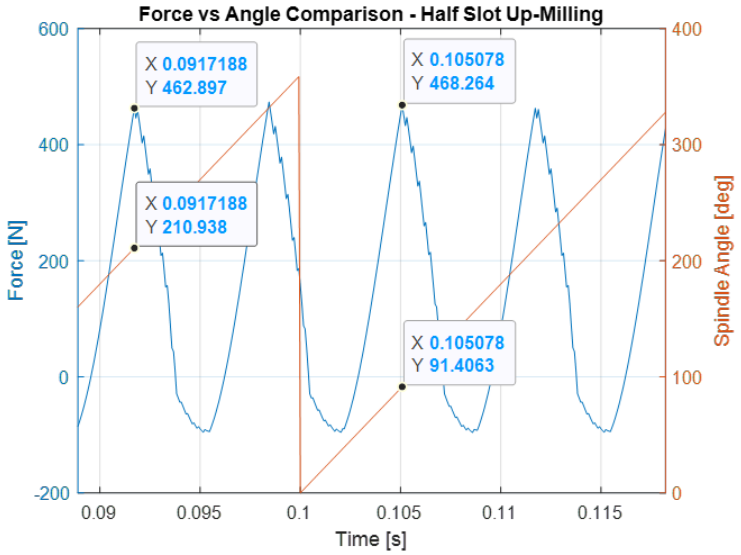

Figure 4.7: Force and Angle Comparison for Half Slot Up Milling

2. For half slot down milling it is seen in Figure 4.8 that the force is zero and at the next step it will start to rise when the angle is 90°.

3. In full slot milling it is seen in Figure 4.9 that the angle is 0° when the force starts to descend.

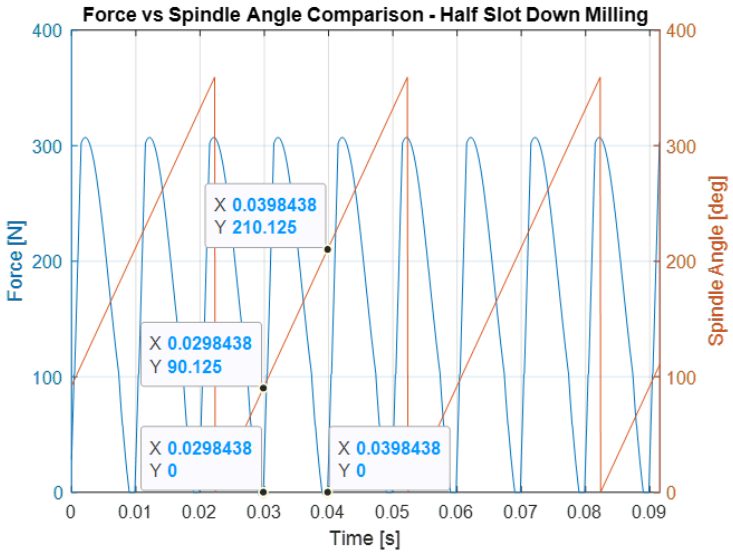

Figure 4.8: Force and Angle Comparison for Half Slot Down Milling

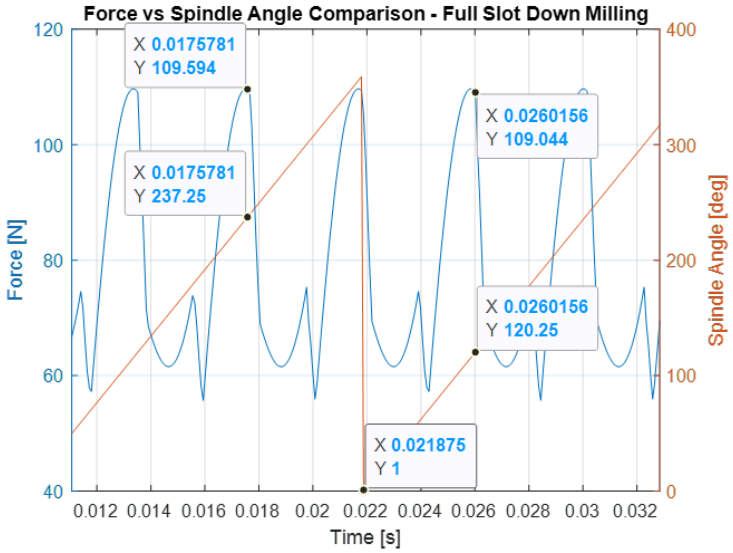

Figure 4.9: Force and Angle Comparison for Full Milling

Before processing the data of real cutting test, the synchronization of angle and force/acceleration data should be done. In each test, the force is plotted. Depending on the type of the cut as explained above, the force peak, force rise or force descend point is selected and its time is noted. At that time, the spindle angle guess is known from the simulation. The acceleration data is processed to start from that time. In ideal conditions, if the force was purely ideal, the desired force point and the

assumed spindle angle should be correct. However, due to measurement noise and dynamometer dynamics, the force is oscillating and it is not possible to exactly select the relevant point for the test. Therefore, a "fine tuning" of the initial spindle angle is needed. If the initial spindle angle is tuned well enough, the force can be estimated.

In the real cutting tests, the need for the initial spindle angle assumption obligated to make some changes in the estimation algorithm given in Figure 3.14. In the algorithm, some sub-steps are added and marked with red in Figure 4.10 to overcome the initial spindle angle necessity. The algorithm with spindle angle assumption update is explained in the following section.

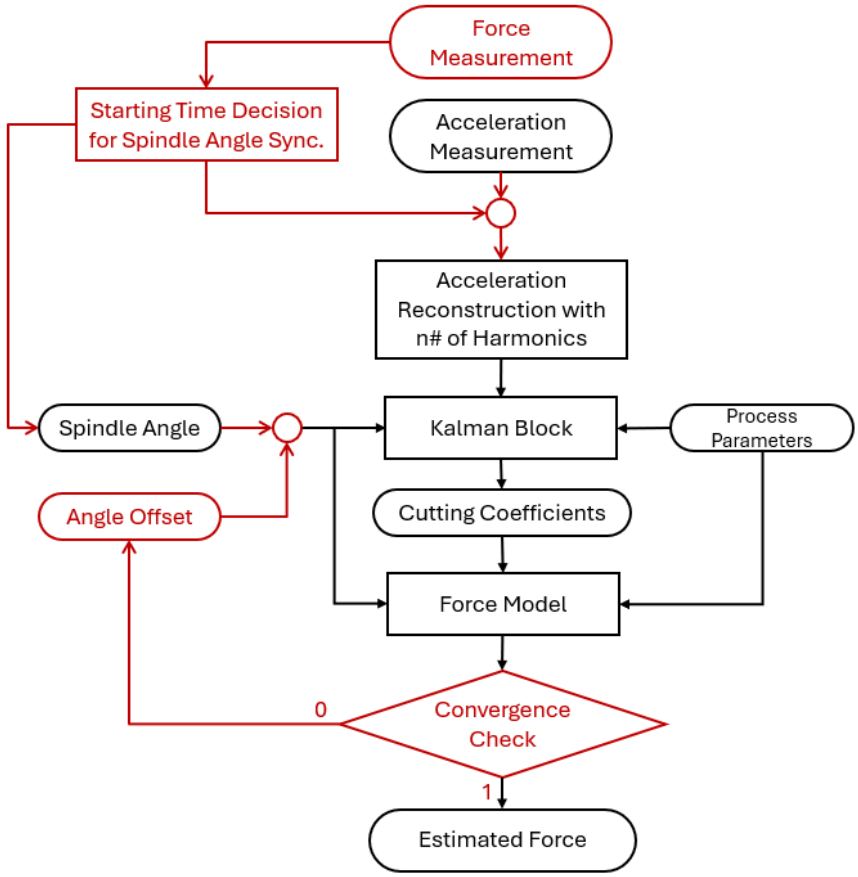

Figure 4.10: Block Diagram of Estimation Algorithm with Spindle Angle Offset

4.3.2 Estimation Algorithm

In previous chapters, it is stated that the estimation part of the work is done offline due to synchronization issues of collected data and spindle angle. In addition, as mentioned in the assumptions, the shift in the time-based acceleration data also contradicts with the measurement matrix modeling. Therefore, there occurs a need for the reconstruction of acceleration data before the estimation algorithm runs. In the previous subsection, the initial spindle angle assumption was discussed. During the decision steps of initial spindle angle, the starting time of the collected data was noted for each test. The estimation algorithm starts with the reconstruction of acceleration data starting from the time value decided for the initial spindle angle. The measured acceleration data starting from the specified time is divided into its harmonics using the FFT algorithm. Next, twenty of its harmonics are converted into time-domain data with an IFFT algorithm. Twenty harmonics is chosen empirically but it can be changed depending on the cutting conditions. For the scope of this thesis, twenty harmonics can cover all the tests conducted in this work. After this process, the time shift of the acceleration data is eliminated. Moreover, this operation also provides to naturally eliminate the structural vibration in the original data. Reconstructed acceleration data, pre-determined Kalman parameters as in Table 4.3, spindle angle whose initial value was decided at the beginning of the algorithm and process parameters are given into the Kalman block. It includes the measurement matrix of the system which combined the force model and workpiece FRF to reflect the milling dynamics. The Kalman block adjusts the state matrix which consists of the cutting coefficients and outputs an estimated acceleration. The estimated acceleration can be compared with the reconstructed acceleration. Besides, the Kalman block outputs the adjusted temporal cutting coefficients for the ill-posed system. Those temporal cutting coefficients are used to calculate the estimated force by using the Eqn. 2.38. If the estimated force is diverged, the fine tuning should be re-done for the spindle angle and the estimation block of Kalman is re-run. When the spindle angle is truly tuned, the algorithm gives the estimated force. The estimated force can be compared with the dynamometer force.

4.3.3 Cutting Test Results

In order to follow a controlled path for validation, the tests are planned group by group. In the first group the tests are conducted with more sensitive impact hammer (Hammer 1) and the 12 mm diameter cutting tool with 3 number of teeth. With independently selected cutting type, spindle speed, feed rate, radial and axial depth of cuts, the cutting tests are utilized. After, the second cutting group is established by changing the impact hammer. The less sensitive impact hammer (Hammer 2) covers a wider frequency range. The sensitivities of the impact hammers was given in Table 4.2. The tipping points are shown in Figure 4.11. The magnitude plots for two hammers are plotted for comparison in Figure 4.12 with the coherence.

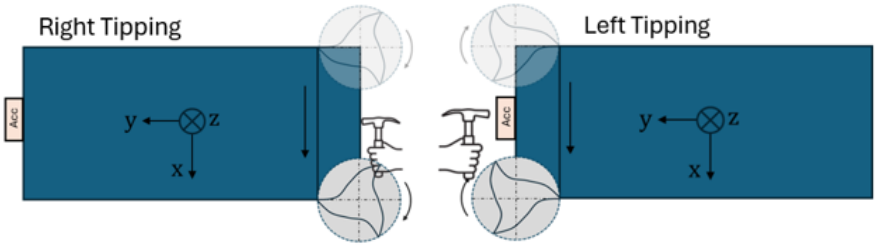

(a) Tipping Direction with Hammer 1 (b) Tipping Direction with Hammer 2

Figure 4.11: Tipping Directions from Top View

Furthermore, the third group is set by changing the cutting tool. In this group the tests are done with a larger diameter cutting tool with the same number of teeth. Lastly, in the forth test group, the cutting diameter is hold the same but the number of teeth is increased to 4. The tool properties are seen in Table 4.4. The list of tests are summarized in Table 4.5.

Table 4.4: Cutting Tool List

Parameter	**Tool 1**	**Tool 2**	**Tool 3**
Diameter	12 mm	16 mm	16 mm
Number of Teeth	3	3	4
Helix Angle	45°	45°	45°

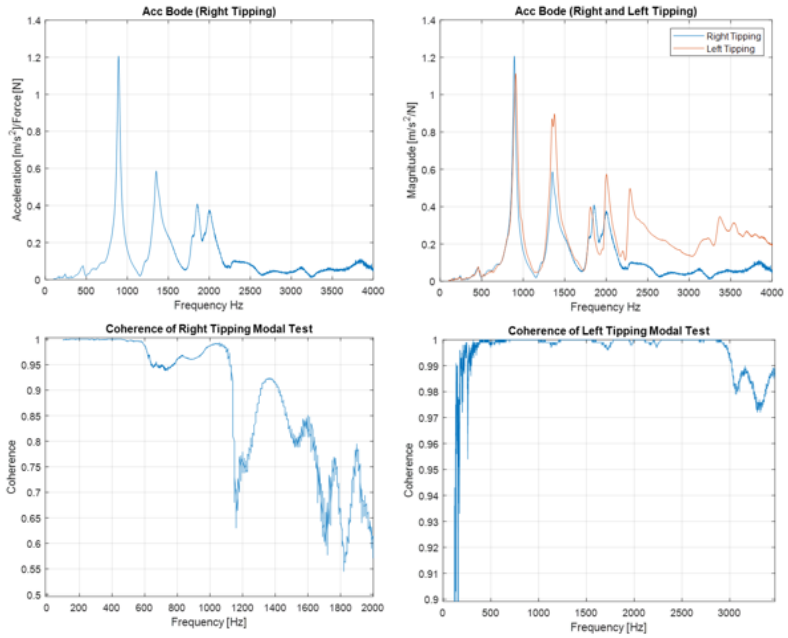

(a) Modal Test with Hammer 1 (b) Modal Test with Hammer 2

Figure 4.12: Modal Test Results for Two Hammers

Table 4.5: Description of the Cutting Tests

Test ID	**Impact Hammer**	**Cutting Tool**	**Milling Type**	**Spindle Speed [rpm]**	**Feed Speed [mm/min]**	**Axial Depth [mm]**	**Radial Depth [mm]**
1	1	1	Down	4500	1500	2	6
2	1	1	Full	4800	1500	1	12
3	1	1	Down	3000	1000	2	6
4	2	1	Full	2000	1500	2	12
5	2	1	Full	2500	1500	2	12
6	2	1	Up	3000	1800	4	6
7	2	2	Full	2400	1000	3	16
8	2	2	Full	4800	500	4	16
9	2	2	Down	2400	500	11	2
10	2	3	Down	3000	1000	3	8
11	2	3	Down	3000	1500	1	8
12	2	3	Down	2400	1200	1	8

In the results starting from Figure 4.13 to Figure 4.24, for each test, the frequency content of force and acceleration data is plotted in Figure (a)'s. This should be done to check whether the test is valid in terms of the assumptions made. The dominant frequencies are expected to be at the tooth passing frequencies. Any harmonics at spindle frequency means that a run-out at the spindle exists. After, original acceleration and reconstructed acceleration are plotted together in Figure (b)'s. It is done to validate the acceleration reconstruction is made correctly. These are the process of the collected data. Next, the estimation algorithm is run and the estimated acceleration is compared with the reconstructed acceleration in Figure (c)'s. The estimation acceleration is calculated based on the acceleration model and the adjusted cutting coefficients. To check their convergence, in Figure (d)'s the temporal cutting coefficients are given. This plot shows whether the estimation algorithm worked correctly. Lastly, in Figure (e)'s, the estimated force calculated using the temporal cutting coefficients is plotted and compared with the measured force. It should be noted that the dynamometer force which is marked as "Dyno Force" at the plot, contains the dynamometer dynamics and measurement noise. Finally, in the Figure (f)'s, the numerical percentage errors of peak, anti-peak if exists and RMS values are compared. Peak value is the maximum value of the force. Anti-peak values are the minimum force value seen in full slot tests. In half slot tests, since the minimum force is zero when the dynamometer harmonics neglected, anti-peak values are not included for half slot tests in comparison tables. RMS values give information about the force profile. Although peaks and anti-peaks match, RMS can differ when the force profile is different. For those results, it should be realized that some of the dominant harmonics did not match with the measured ones.

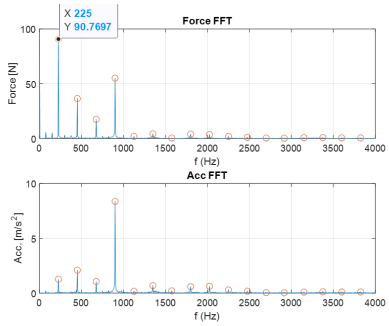

(a) Frequency Contents of Force and Acceleration

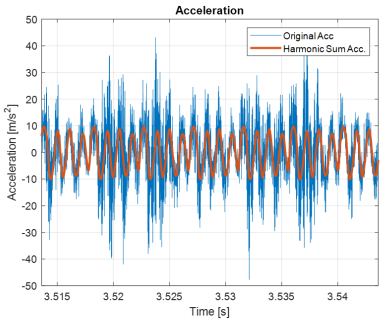

(b) Reconstructed Acceleration Comparison

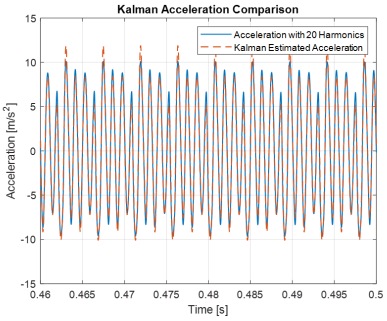

(c) Estimated Acceleration Comparison

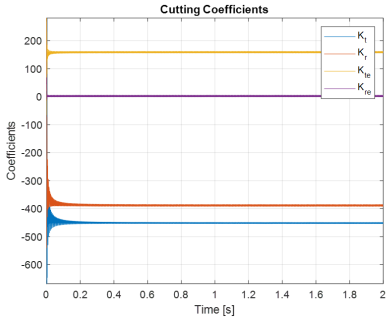

(d) Temporal Cutting Coefficients

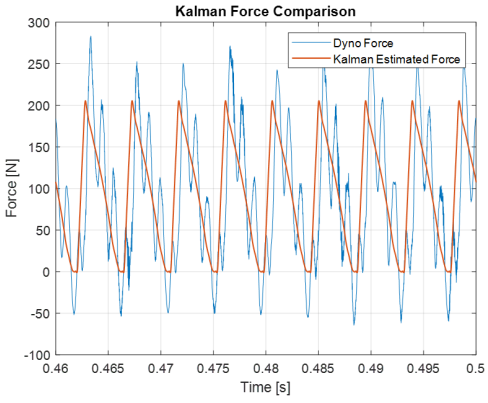

(e) Estimated Force

Parameter	Dyno Force	Estimated Force
Peak Value	217.1	205.4
Peak Error	-	5.4 %
RMS	114.4	108.8
RMS Error	-	4.8 %

(f) Error Percentages

Figure 4.13: Results of Test 1 D12 N3 S4500 f1500 ap2 ae6

In Test 1, Figure 4.13, when looked into the frequency content of the acceleration, the most dominant harmonic is around the natural frequency of the workpiece as seen in modal test results, Figure 4.12. Also in Figure 4.4, it was seen that the FRF results are inconsistent around the natural frequencies due to the movement of the spindle during the cut. In this test, the dominant frequency component of the acceleration is around the natural frequency however the inconsistency of the FRF at the first mode is around 25% at its maximum which is not a big problem for that mode. As a result, although the first mode is perturbed, since the deviation of FRF is not high, the estimated force error percentages came around 5% which can be accepted as an accurate result compared to the literature. However, it should be noted that the natural frequencies are the dangerous regions due to the variable FRF gains. The acceleration and the force is estimated and it highly matches with the reconstructed and measured values. The cutting coefficients are converged but their values are not physical due to the ill-posed situation between acceleration and force.

In Test 2, Figure 4.14, when looked into the frequency content of the acceleration, the most dominant harmonic is again around the natural frequency but the mode is not directly perturbed. If the algorithm has run directly with the collected acceleration data, the dominance of natural vibrations would cause the algorithm to diverge because the model does not include the frequency components other than the tooth passing frequencies. In this test, the importance of the acceleration reconstruction can be seen. Since it is a full slot test, one should realize that there is a minimum point of the force which is called anti-peak value in comparison table. With the truly tuned spindle angle, the error percentages are less than 10% and the cutting coefficients are more physical due to the large force offset and the minimum value.

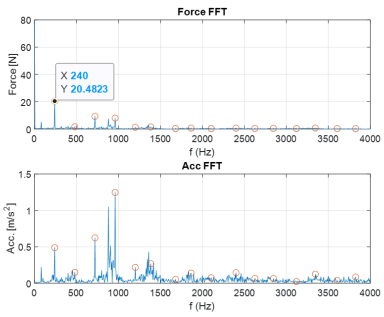

(a) Frequency Contents of Force and Acceleration

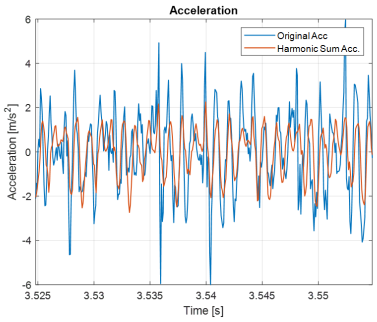

(b) Reconstructed Acceleration Comparison

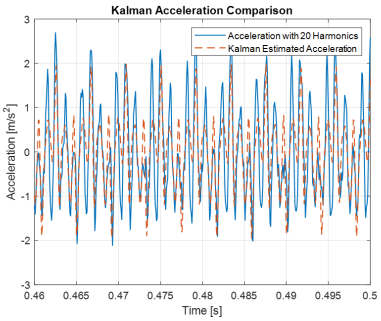

(c) Estimated Acceleration Comparison

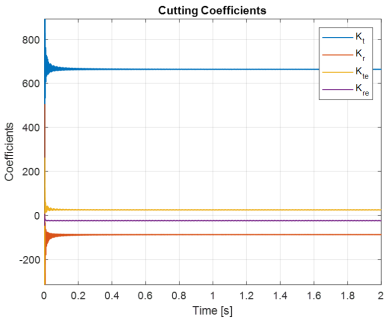

(d) Temporal Cutting Coefficients

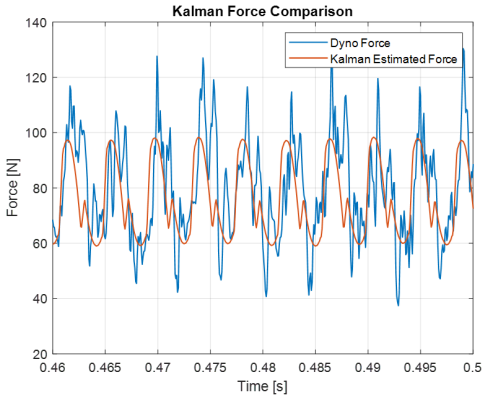

(e) Estimated Force

Parameter	Dyno Force	Estimated Force
Peak Value	106.7	97.8
Peak Error	-	8.3 %
Anti Peak Value	55.8	59.2
Anti Peak Err.	-	6.1 %
RMS	76.8	77.8
RMS Error	-	1.3 %

(f) Error Percentages

Figure 4.14: Results of Test 2 D12 N3 S4800 f1500 ap1 ae12

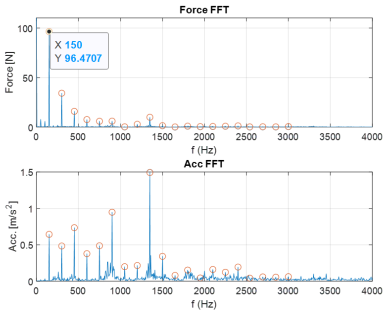

(a) Frequency Contents of Force and Acceleration

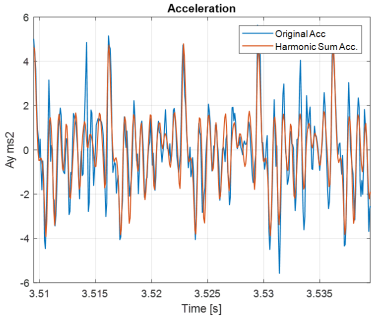

(b) Reconstructed Acceleration Comparison

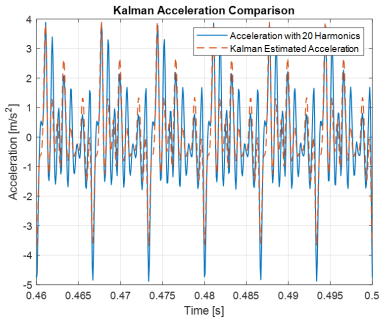

(c) Estimated Acceleration Comparison

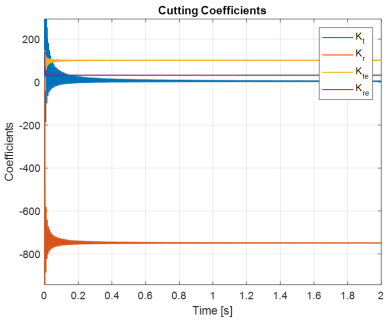

(d) Temporal Cutting Coefficients

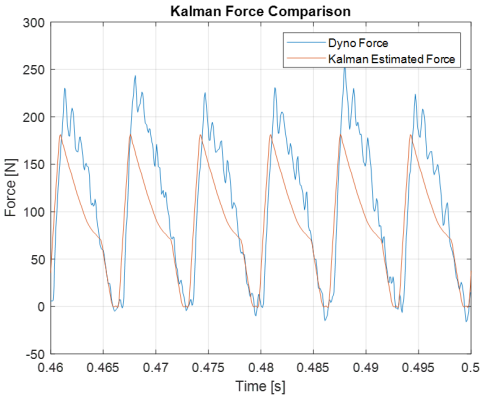

(e) Estimated Force

Parameter	Dyno Force	Estimated Force
Peak Value	226.3	181.4
Peak Error	-	19.8 %
RMS	131.3	103.0
RMS Error	-	21.6 %

(f) Error Percentages

Figure 4.15: Results of Test 3 D12 N3 S3000 f1000 ap2 ae6

In Test 3, Figure 4.15, when looked into the frequency content of the acceleration, the most dominant harmonics are around the two natural frequencies of the workpiece as seen in modal test results, Figure 4.12. Also in Figure 4.4, it was seen that the FRF results are inconsistent around the natural frequencies due to the movement of the spindle during the cut especially in the second mode. In this test, the dominant frequency component of the acceleration is around the second natural frequency and the inconsistency of the FRF at the second mode is more than 60%. That huge error diverged the results from the real values. Despite the FRF inconsistency, force-model based algorithm tried to be near the mathematical values of force depending on the pre-known process variables. With the non-physical values of adjusted cutting coefficients the force errors become about 20% of the measured ones.

In Test 4, Figure 4.16, the modal test results changed. The hammer used in this test is less sensitive but it covers a wider frequency range. When looked into the frequency content of the acceleration, the most dominant harmonic is around the second natural frequency but the mode is not directly perturbed. If the algorithm has run directly with the collected acceleration data, the dominance of natural vibrations would cause the algorithm to diverge because the model does not include the frequency components other than the tooth passing frequencies. It is a full slot test, therefore as mentioned before, the cutting coefficients are more physical due to the large force offset and the minimum value. With the truly tuned spindle angle, the error percentages are less than 10%. The effect of hammer change is seen in the first harmonics since the coherence values are lower in lower frequencies (lower than 500 Hz) as seen in Figure 4.12. The cause of the increasing error is the deviations in the first harmonics.

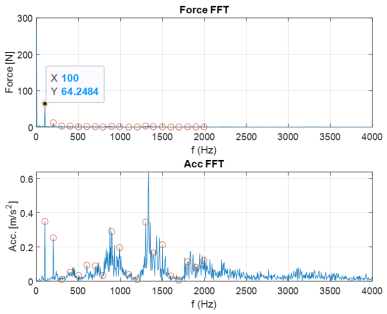

(a) Frequency Contents of Force and Acceleration

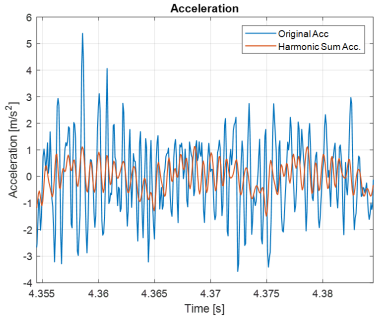

(b) Reconstructed Acceleration Comparison

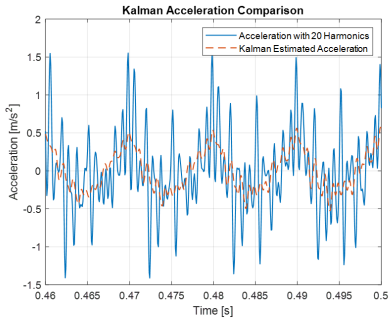

(c) Estimated Acceleration Comparison

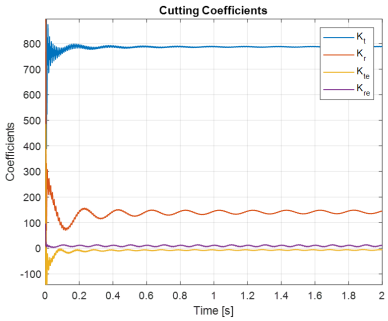

(d) Temporal Cutting Coefficients

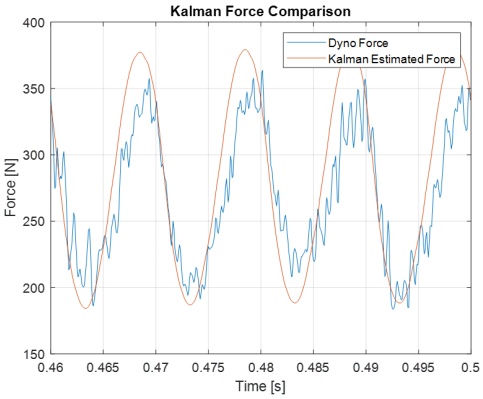

(e) Estimated Force

Parameter	Dyno Force	Estimated Force
Peak Value	348.0	379.3
Peak Error	-	9.0 %
Anti Peak Value	206.0	186.8
Anti Peak Err.	-	9.3 %
RMS	268.1	288.1
RMS Error	-	7.5 %

(f) Error Percentages

Figure 4.16: Results of Test 4 D12 N3 S2000 f1500 ap2 ae12

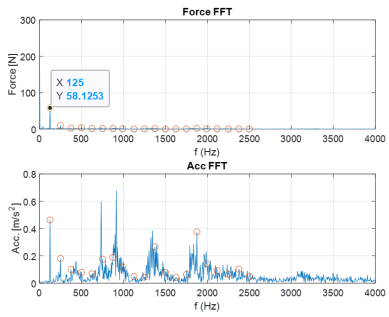

(a) Frequency Contents of Force and Acceleration

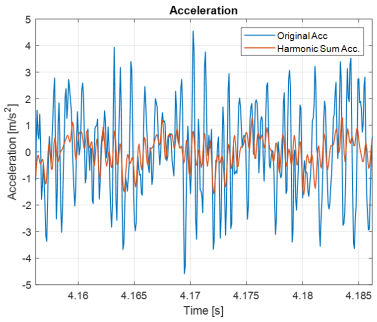

(b) Reconstructed Acceleration Comparison

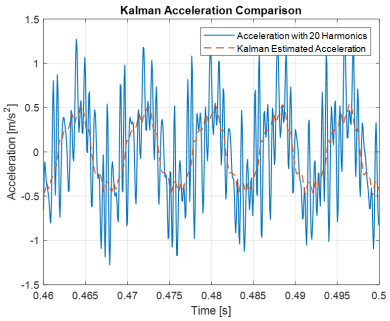

(c) Estimated Acceleration Comparison

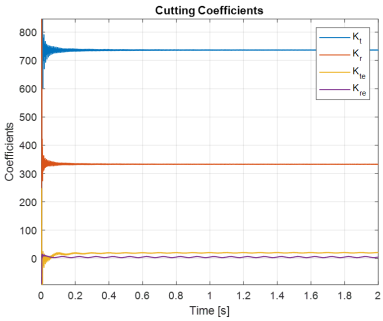

(d) Temporal Cutting Coefficients

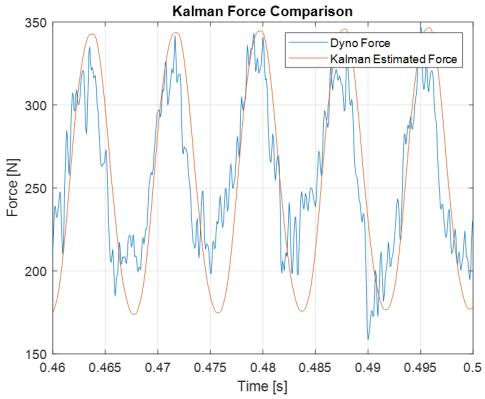

(e) Estimated Force

Parameter	Dyno Force	Estimated Force
Peak Value	329.8	342.8
Peak Error	-	3.9 %
Anti Peak Value	176.2	174.9
Anti Peak Err.	-	0.7 %
RMS	264.1	263.9
RMS Error	-	0 %

(f) Error Percentages

Figure 4.17: Results of Test 5 D12 N3 S2500 f1500 ap2 ae12

In Test 5, Figure 4.17, when looked into the frequency content of the acceleration, the most dominant harmonic is the first harmonic. The components due to natural vibrations, in other words, the frequency contents of the acceleration around the natural frequencies, are not perturbed. The acceleration content is crowded due to natural vibrations. The acceleration reconstruction provided them to be eliminated in the estimation algorithm. The relevant acceleration harmonics are used to find the relevant force harmonics with the consistent part of the FRF results. It is a full slot test, therefore as mentioned before, the cutting coefficients are more physical due to the large force offset and the minimum value. As a result of those, the error percentage values are less than 4% and an accurate force estimation is utilized for this test.

In Test 6, Figure 4.18, when looked into the frequency content of the acceleration, the most dominant harmonics are around the two natural frequencies of the workpiece as seen in modal test results, Figure 4.12. Also in Figure 4.4, it was seen that the FRF results are inconsistent around the natural frequencies due to the movement of the spindle during the cut especially in the second mode. In this test, the dominant frequency components of the acceleration are around the two natural frequencies and the inconsistency of the FRF at the second mode is more than 60%. The huge error in the FRF increased the error between measured force and the estimated force. Two dominant natural frequency components prevented the algorithm from using the remaining components for estimation. With the non-physical values of adjusted cutting coefficients the force errors become more than 20%. From the results, it is realized that the frequency interval of interest should be away from the natural frequencies of the workpiece. The mode shapes should not be perturbed since the amplitude gains cannot be predicted correctly especially when they are dominating.

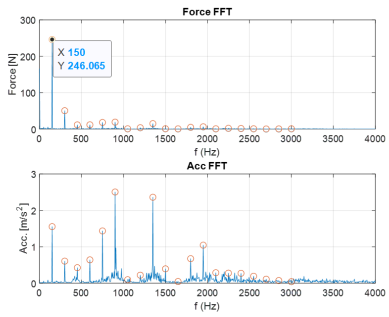

(a) Frequency Contents of Force and Acceleration

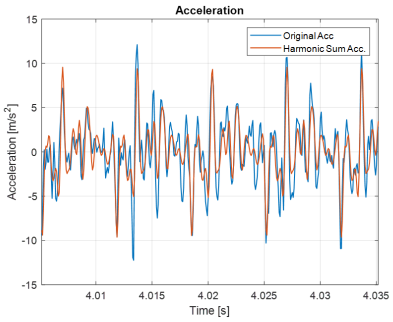

(b) Reconstructed Acceleration Comparison

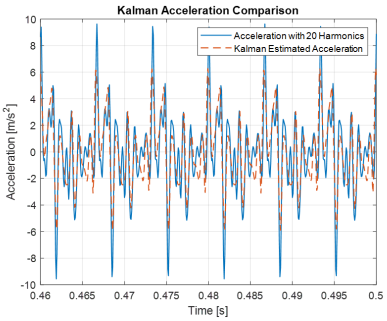

(c) Estimated Acceleration Comparison

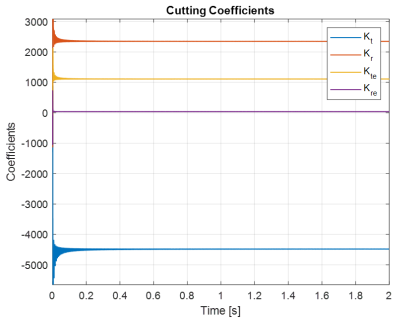

(d) Temporal Cutting Coefficients

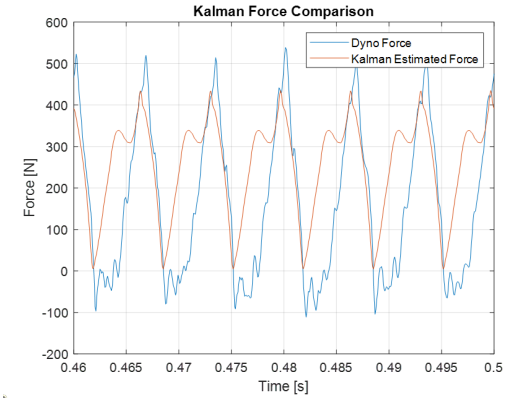

(e) Estimated Force

Parameter	Dyno Force	Estimated Force
Peak Value	514.3	434.0
Peak Error	-	15.6 %
RMS	220.1	283.1
RMS Error	-	28.6 %

(f) Error Percentages

Figure 4.18: Results of Test 6 D12 N3 S3000 f1800 ap4 ae6

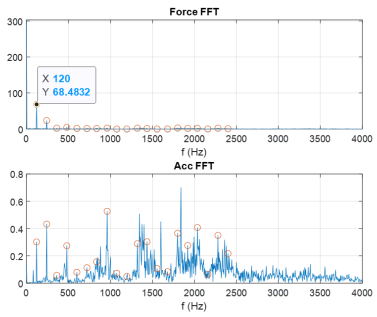

(a) Frequency Contents of Force and Acceleration

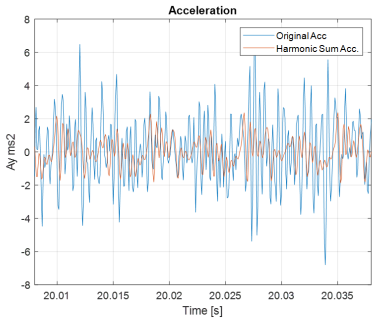

(b) Reconstructed Acceleration Comparison

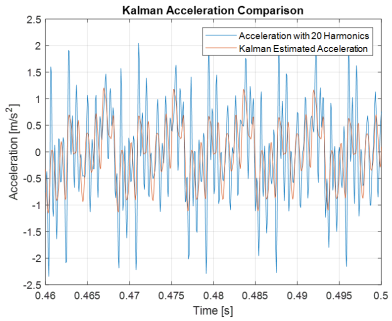

(c) Estimated Acceleration Comparison

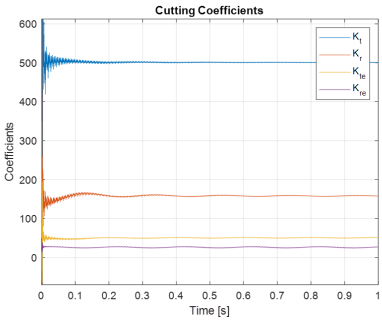

(d) Temporal Cutting Coefficients

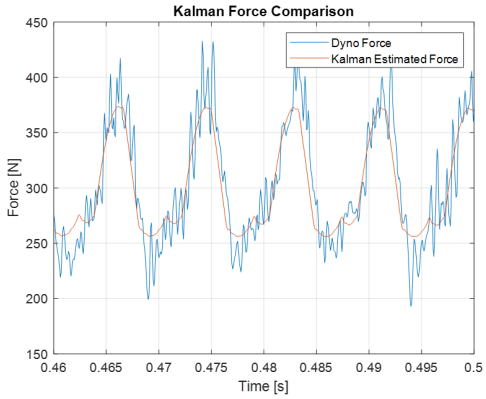

(e) Estimated Force

Parameter	Dyno Force	Estimated Force
Peak Value	389.6	373.7
Peak Error	-	4.3 %
Anti Peak Value	242.8	256.5
Anti Peak Err.	-	5.3 %
RMS	307.8	303.8
RMS Error	-	1.3 %

(f) Error Percentages

Figure 4.19: Results of Test 7 D16 N3 S1400 f1000 ap3 ae16

In Test 7 and Test 8, Figure 4.19 and 4.20, the cutting tool diameter has changed. There is no obvious effect of diameter change in terms of the estimation accuracy. When looked into the frequency content of the acceleration, a balanced acceleration profile is seen for both tests. The mode shapes are not perturbed. For the elimination

of high frequency natural vibrations, the acceleration reconstruction is a helpful. They are full slot tests, therefore the cutting coefficients are more physical due to the large force offset and the minimum value. Their values are estimated very close to each other. With the truly tuned spindle angle, the error percentages are less than 5%.

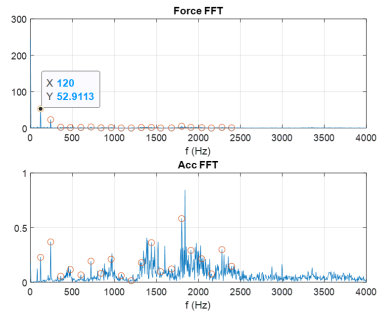

(a) Frequency Contents of Force and Acceleration

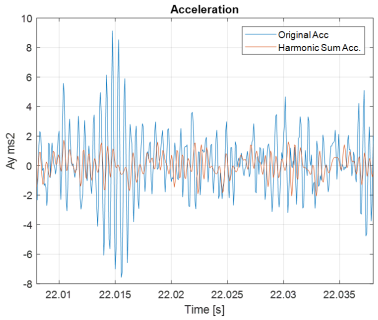

(b) Reconstructed Acceleration Comparison

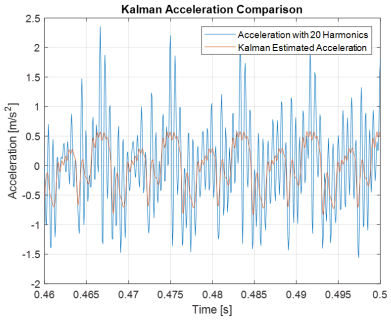

(c) Estimated Acceleration Comparison

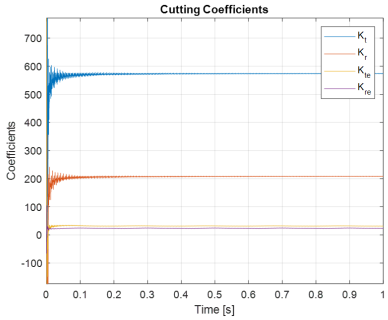

(d) Temporal Cutting Coefficients

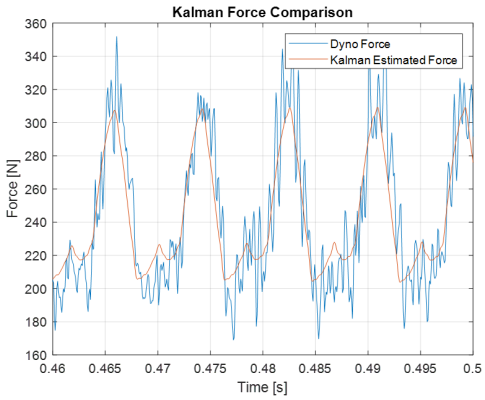

(e) Estimated Force

Parameter	Dyno Force	Estimated Force
Peak Value	315.4	309.0
Peak Error	-	2.1 %
Anti Peak Value	197.2	205.1
Anti Peak Err.	-	3.9 %
RMS	249.5	256.2
RMS Error	-	2.6 %

(f) Error Percentages

Figure 4.20: Results of Test 8 D16 N3 S2400 f500 ap4 ae16

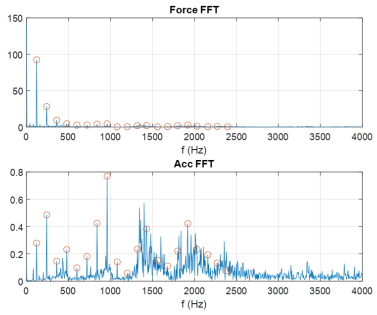

(a) Frequency Contents of Force and Acceleration

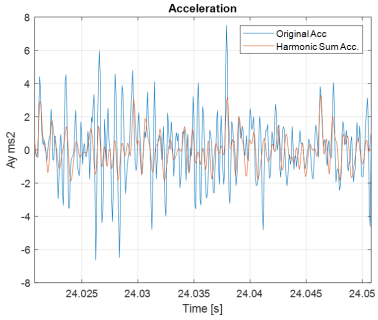

(b) Reconstructed Acceleration Comparison

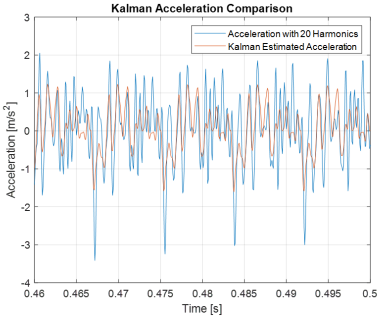

(c) Estimated Acceleration Comparison

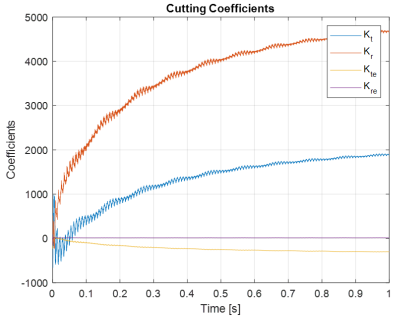

(d) Temporal Cutting Coefficients

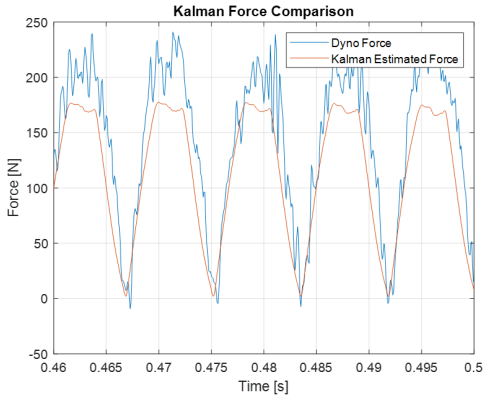

(e) Estimated Force

Parameter	Dyno Force	Estimated Force
Peak Value	199.4	174.0
Peak Error	-	12.7 %
RMS	159.9	125.4
RMS Error	-	21.5 %

(f) Error Percentages

Figure 4.21: Results of Test 9 D16 N3 S2400 f500 ap11 ae2

In Test 9, Figure 4.21, when looked into the frequency content of the acceleration, the most dominant harmonic is the first natural frequency of the workpiece as seen in modal test results, Figure 4.12. The other frequency content of acceleration is balanced. The second and even the third natural frequency contribute the same as the first two harmonics. In Figure 4.12, it was seen that the FRF results are inconsistent around the second natural frequency due to the movement of the spindle during the cut. Moreover, as seen in Figure 4.12, the coherence of the low frequency components are lower. The low consistency of first natural frequency, inconsistency of the second natural frequency and the lower coherence in lower frequencies caused the error percentage to increase in this test. With the non-physical values of adjusted cutting coefficients the force errors become around 20%.

In Test 10, Figure 4.22, the number of teeth of the cutting tool increased to 4 from 3. When there are 3 teeth, the angle between them is 120°. During a half slot cutting test, which the difference between entrance and exiting angles is 90°, for a time interval the tooth and workpiece interaction cancels for that 30° difference. However, in 4 teeth cutting tool, the interaction always continues. When looked into the frequency content of the acceleration, the tooth passing frequencies are the dominant components compared to the natural vibration of the workpiece. There always exists a force that perturbs the workpiece. In this test, a high frequency component is amplified which may cause due to dynamometer dynamics. Since it is not one of the orders of the tooth passing frequency, it is not included in the acceleration thanks to the acceleration reconstruction. Due to the dominance of force harmonics and consistent dominant FRF, the estimation errors are less than 4%. The force is predicted with high accuracy.

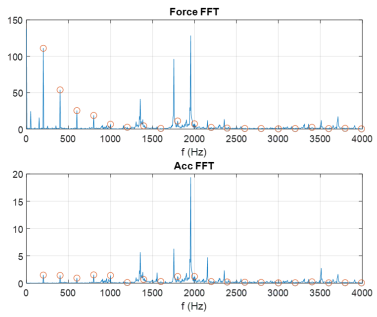

(a) Frequency Contents of Force and Acceleration

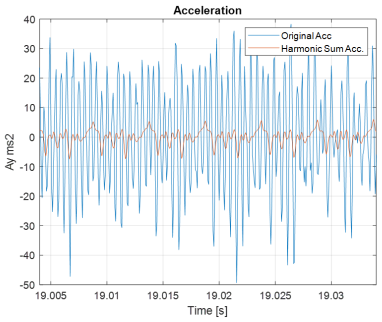

(b) Reconstructed Acceleration Comparison

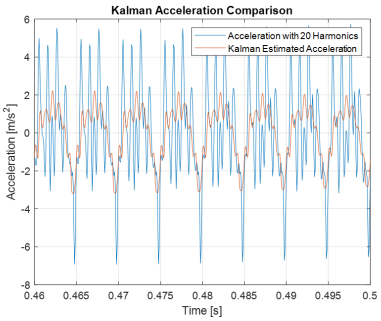

(c) Estimated Acceleration Comparison

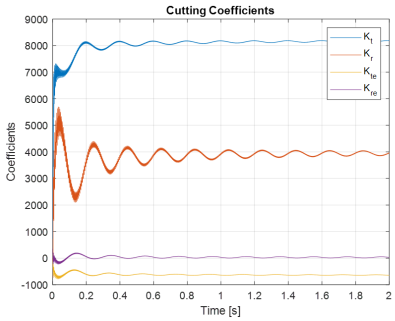

(d) Temporal Cutting Coefficients

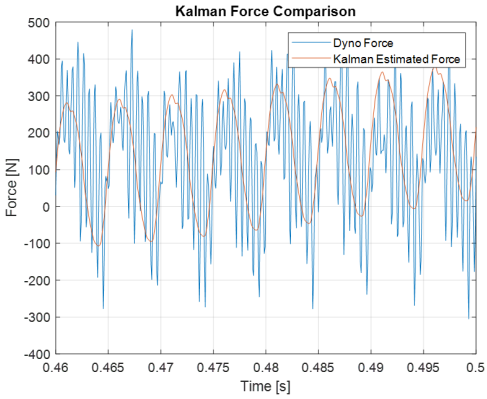

(e) Estimated Force

Parameter	Dyno Force	Estimated Force
Peak Value	293.4	302.7
Peak Error	-	3.2 %
RMS	211.9	203.4
RMS Error	-	4.0 %

(f) Error Percentages

Figure 4.22: Results of Test 10 D16 N4 S3000 f1000 ap3 ae8

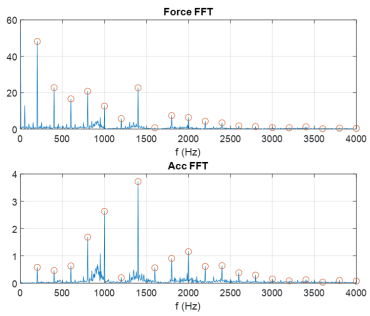

(a) Frequency Contents of Force and Acceleration

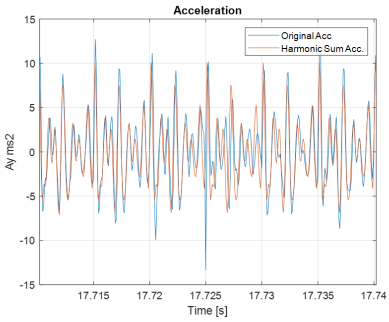

(b) Reconstructed Acceleration Comparison

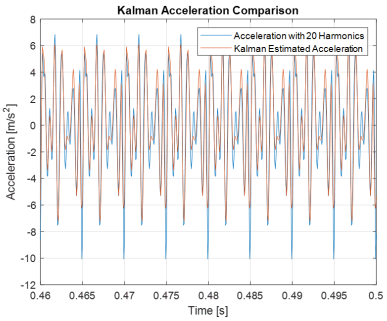

(c) Estimated Acceleration Comparison

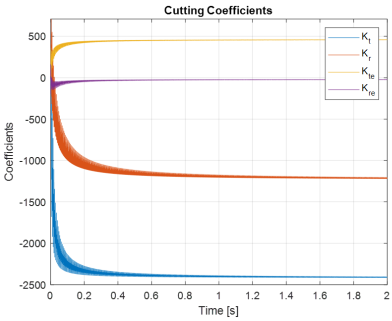

(d) Temporal Cutting Coefficients

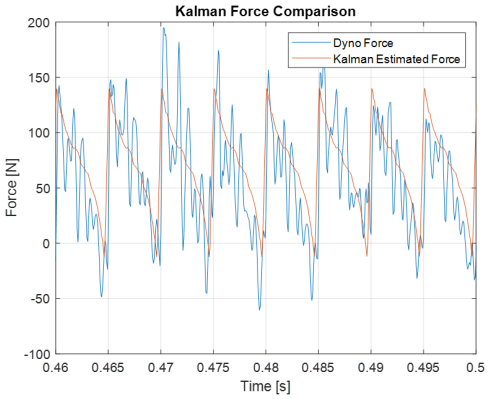

(e) Estimated Force

Parameter	Dyno Force	Estimated Force
Peak Value	145.3	139.8
Peak Error	-	3.7 %
RMS	76.2	80.4
RMS Error	-	5.5 %

(f) Error Percentages

Figure 4.23: Results of Test 11 D16 N4 S3000 f1500 ap1 ae8

In Test 11 and Test 12, Figure 4.23 and 4.24, different from the Test 10, there is no high frequency structural component of the acceleration. Due to the continuous tooth and workpiece interaction, the tooth passing frequencies are the dominant components compared to the structural vibration of the workpiece. There always exists a

force that perturbs the workpiece. Due to the dominance of force harmonics and consistent dominant FRF, the estimation errors are less than 5%. The force is predicted with high accuracy.

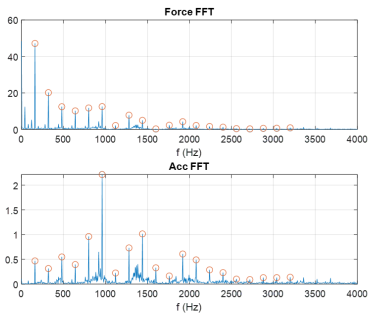

(a) Frequency Contents of Force and Acceleration

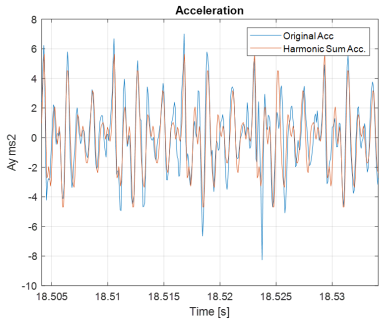

(b) Reconstructed Acceleration Comparison

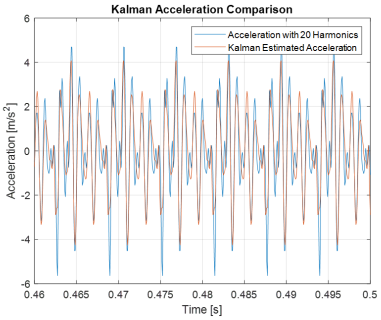

(c) Estimated Acceleration Comparison

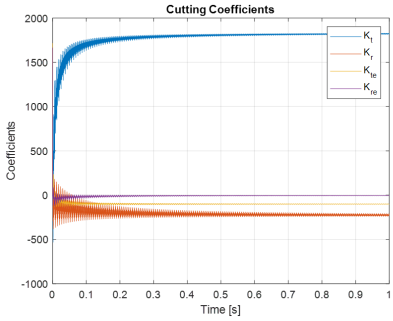

(d) Temporal Cutting Coefficients

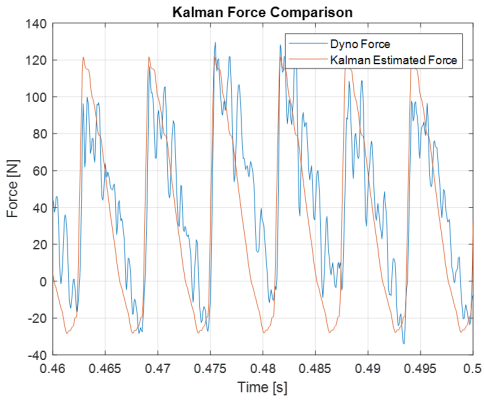

(e) Estimated Force

Parameter	Dyno Force	Estimated Force
Peak Value	121.8	120.6
Peak Error	-	0.9 %
RMS	60.0	61.2
RMS Error	-	2 %

(f) Error Percentages

Figure 4.24: Results of Test 12 D16 N4 S2400 f1200 ap1 ae8

Table 4.6: Comparison of Dynamometer and Estimated Forces Across Tests

	Test ID 1		**Test ID 2**		**Test ID 3**	
Parameter	**Dyno Force [N]**	**Estimated Force [N]**	**Dyno Force [N]**	**Estimated Force [N]**	**Dyno Force [N]**	**Estimated Force [N]**
Peak Value	217.1	205.4	106.7	97.8	226.3	181.4
Peak Error	-	5.4%	-	8.3%	-	19.8%
RMS	114.4	108.8	76.8	77.8	131.3	103
RMS Error	-	4.8%	-	1.3%	-	21.6%
Anti Peak Value	N/A	N/A	55.8	59.2	N/A	N/A
Anti Peak Error	N/A	N/A	-	6.1%	N/A	N/A
	Test ID 4		**Test ID 5**		**Test ID 6**	
Parameter	**Dyno Force [N]**	**Estimated Force [N]**	**Dyno Force [N]**	**Estimated Force [N]**	**Dyno Force [N]**	**Estimated Force [N]**
Peak Value	348	379.3	329.8	342.8	514.3	434
Peak Error	-	9.0%	-	3.9%	-	15.6%
RMS	268.1	288.1	264.1	263.1	220.1	283.1
RMS Error	-	7.5%	-	0.0%	-	28.6%
Anti Peak Value	206	186.8	176.2	174.9	N/A	N/A
Anti Peak Error	-	9.3%	-	0.7%	N/A	N/A
	Test ID 7		**Test ID 8**		**Test ID 9**	
Parameter	**Dyno Force [N]**	**Estimated Force [N]**	**Dyno Force [N]**	**Estimated Force [N]**	**Dyno Force [N]**	**Estimated Force [N]**
Peak Value	389.6	373.7	315.4	309	199.4	174
Peak Error	-	4.3%	-	2.1%	-	12.7%
RMS	307.3	303.8	249.5	256.2	159.9	125.4
RMS Error	-	1.3%	-	2.6%	-	21.5%
Anti Peak Value	242.8	256.5	197.2	202.5	N/A	N/A
Anti Peak Error	-	5.3%	-	3.9%	N/A	N/A
	Test ID 10		**Test ID 11**		**Test ID 12**	
Parameter	**Dyno Force [N]**	**Estimated Force [N]**	**Dyno Force [N]**	**Estimated Force [N]**	**Dyno Force [N]**	**Estimated Force [N]**
Peak Value	293.4	302.7	145.3	139.8	121.8	120.6
Peak Error	-	3.2%	-	3.7%	-	0.9%
RMS	211.9	203.4	76.2	80.4	60.0	61.2
RMS Error	-	4%	-	5.5%	-	2.0%
Anti Peak Value	N/A	N/A	N/A	N/A	N/A	N/A
Anti Peak Error	N/A	N/A	N/A	N/A	N/A	N/A

The results are collected in Table 4.6. In each cutting case, the peak force values of both the measured and estimated ones are compared. It is vital to estimate the maximum force during a cutting operation. For half-slot tests, when the further harmonics are neglected, the minimum force is nominally zero. Therefore for half slot tests the minimum values are not compared. However, in full slot tests, the force behavior is different. It has a mean value and includes the magnitudes of harmonics. In full slot tests, the maximum and minimum force values exist. For that reason, peak and anti-peak values are compared for full slot cases. Besides the minimum and maximum force values, the force profile should be checked. Although the peak values of the forces match each other, the types of oscillations may differ. To check this, RMS values of the forces in a specific time period are calculated and tabulated. The percentage values of error are given in Figure 4.25. X axis is the Test ID's and Y axis is the percentage error in %. The first columns are the peak errors, the second ones are the RMS errors and the third one is the anti peak errors for full slot cutting tests. In order to increase the perception, a constant line is drawn at 10% error because when compared with the literature work, that 10% error value is accepted as a successful value among the estimation algorithms.

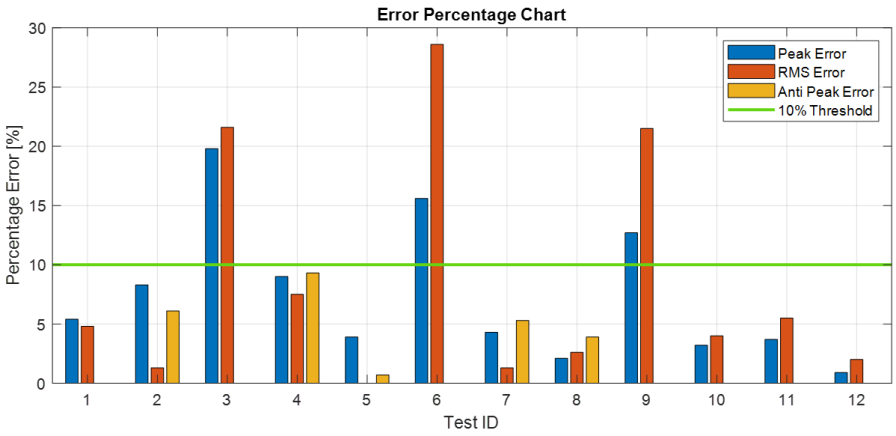

Figure 4.25: Error Percentages of Cutting Tests

4.4 Discussion

By examining the overall results, the average error percentage of this work is between 5-10%. Comparing with the literature work, the proposed algorithm seem to be a good alternative for indirect force estimation. However, the error of three of the twelve cutting tests are higher than the others. The possible reasons beyond this will be discussed in this section. For the Test 3, the results are examined by looking at Figure 4.15. When the frequency content is checked, it can be seen that the first two dominant acceleration harmonics are around the natural frequencies of the workpiece as in FRF plots, 4.12. In the frequency content of the acceleration, those dominant modes are perturbed either with force component or naturally, in other words, the magnitudes of the acceleration in natural frequencies can be due to cutting force and due to structural vibration. The FRF result gives the relation between the force and acceleration. However, like in Figure 4.4, as the spindle moves along the workpiece, although the FRF is very stable over the frequency range, in natural frequencies the magnitude values change significantly. As the FRF value is not exact in the dominant acceleration frequencies especially in natural frequencies, the algorithm did not work successfully as the other cases. Moreover, the modal test of this case was done with highly sensitive but covering a narrower frequency range hammer. As a result of those, the accuracy of the test decreased. When looked at the Test 6, it is seen that the same scenario happened. The effect of the structural vibration and force contribution cannot be separated. The algorithm could not find the contribution of the force harmonics at the dominant frequencies which are natural frequencies. As a result of this, the first harmonic contribution did not match with the real one. Consequently, the error percentage values increased. In Test 9, the common reasons cause the force estimation value differ from the expected value. The mutuality between those three tests with higher error percentage values is that they all are kind of half slot tests. In actual, Test 3 and 6 are directly half slot tests. In Test 9, the radial depth is less than the radius of the tool but the force behavior is similar to the half slot cuts. A mismatch of the force harmonics at the dominant acceleration frequencies, causes the DC component or the first harmonic force of the half slot cut to diverge from the real value. As a result of this, the errors in peak values increase. Moreover, since the force profile changes, the RMS errors increase more. When dived into the Test 7 or 8, which are

full slot tests, although there exist dominant acceleration harmonics around natural frequencies of the workpiece as in Test 3, 6 and 9, the estimated force is not affected badly as much as the half slot tests. In full slot tests, the force profile is different than the half slot ones. In full cutting, the DC component of the force is more dominant and the minimum force value is not zero. The oscillation of the cutting force is does not start from zero as in half slot cutting. When spindle angle is tuned properly, a mismatch in the dominant frequencies causes the DC component and the first harmonic of the force differ from the real value. In that case, due to the nature of the Kalman filter, it continues to iterate for the solution because DC or first harmonic component difference should be compensated. At the end, since the contribution of them is more dominant in full slot tests, the Kalman converges the DC offset and the first harmonic of the force. Therefore, the estimation algorithm works more stable in full slot tests. Even better, the temporal cutting coefficients that the Kalman filter adjusts, are more prone to converge to the real values in full slot tests. The converged values of the coefficients in full slot tests in this thesis are physically relevant. According to the results of the cutting tests, it can be stated that the conducted cutting tests gave a deep insight of the proposed algorithm. The tests are utilized in different and controlled configurations. The error percentages are less than 5% for most of the tests.

CHAPTER 5

CONCLUSIONS

Among the researchers working on milling process, indirect calculation of the cutting force is a popular topic. Using some traditional, statistical, mathematical or technological methods, the cutting force can be estimated. There is huge number of researches that use the same methodologies from their own perspectives. By adding some improvements to the existing methods, the milling process is tried to be improved in the literature. Today, there exist different methods to estimate the cutting forces, but the main challenge has become to find the most accurate force in the fastest and cheapest way. In other words, the researches are mainly focusing on the most simple, cost-effective, accurate, adaptable, robust and easy-implementable solutions. Moreover, the methods are intended to be adapted to online systems and give the estimation in milliseconds with high accuracy. The common idea in the literature is that the accelerometers are the most useful instruments that satisfies most of the requirements to make cutting force estimation. When dived into the research results, the least error percentages are achieved by accelerometer-based methods. Their common usage, ease of mounting and data processing availability made them the first choice. Therefore, the instrument of this thesis is chosen as the accelerometers. The open-for-improvement part of the force estimation became the algorithm.

As a contribution to the literature about force estimation in milling process, this thesis work is managed. Generally, the common methods are used in the literature and tried to do some performance improvements for the common methods. However, in this thesis, a novel method for force estimation is attempted. Different from the previous work, a force-model based algorithm using the Kalman filter is developed. The usage of force model provides a more stable structure against the discrepancies in the

experiments. The force model narrows down the final estimation in a possible interval with the known parameters. To convert this force model to the acceleration, FRF of the workpiece is used which can be acquired easily with an impact hammer. The usage of the FRF is also different from the literature work. The force model provided the harmonics of the force depending on the fact that its components are occurring in tooth passing frequencies. With the help of this, there was no need to make a complex transfer function estimations. Rather, with basic mathematical operations, the dynamics of the workpiece is reflected to the acceleration model. The gains in FRF are multiplied with the amplitude of force harmonics and the phase angle of the FRF is added to the phases of the force harmonics to get the acceleration harmonics. Adapting the acceleration expression derived from force model and FRF to the Kalman filter, a flexibility against the noise is gained in the estimation model. Thanks to the structure, accurate force estimations are done as verified with real cutting tests. Besides its advantages, there are some points that should be improved in the proposed algorithm. One of them is that the model does not include the run-out of the cutter. In the tests, run-out of the spindle is checked at the beginning, however for the method to be used in the industrial applications, run-out effects should be included. Another disadvantage of the model is that a structural vibration elimination process is needed. Since the force model only includes the tooth passing frequency harmonics, the existence of the dominant structural vibrations affect the Kalman in a bad way. The algorithm tries to compensate the non-harmonic terms with the harmonic terms which misguide the results. Lastly, one of the most important issue about the algorithm is that it requires the spindle angle synchronized with the acceleration. The force model, Eqn. 2.38, calculates the force magnitude as a function of spindle angle. Thinking the mechanics of the process, the engagement or the disengagement of the tool and the workpiece is needed accurately. However, in today's technology, it would not be a hard issue to collect spindle angle data synchronized with the acceleration.

Overall, investigating the experiments to verify the method, the proposed method provides valuable insights for force estimation by using a novel approach. The accuracy of the method is high compared to the literature work. With the lessons learned from the real cutting tests, this work is open to be improved and get more stable, accurate estimation results. As the models of force, acceleration, FRF and Kalman blocks

are in discrete domain, the algorithm is applicable for real-time applications. With properly implemented and calibrated instruments and additional signal processing algorithms, more accurate results can be achieved.

REFERENCES

[1] O. W. Boston, W. W. Gilbert, and K. B. Kaiser. Power and forces in milling SAD 3150 with helical mills. *Transactions of the ASME*, 59(2):545–545, 1937.

[2] E. J. A. Armarego and R. H. Brown. *The Machining of Metals*. Prentice-Hall, 1969.

[3] M. E. Martellotti. An analysis of the milling process. *Transactions of the ASME*, 63:677–695, 1941.

[4] F. Koenigsberger and A. J. P. Sabberwal. An investigation into the cutting force pulsations during milling operations. *International Journal of Machine Tool Design and Research*, 1:15–33, 1961.

[5] W. A. Kline, R. E. DeVor, and J. R. Lindberg. The prediction of cutting forces in end milling with application to cornering cuts. *International Journal of Machine Tool Design and Research*, 22(1):7–22, 1982. 10.1016/0020-7357(82)90016-6.

[6] Jiunn-jyh Junz, Steven Y. Wang, Wayne J. Book. Convolution Analysis of Milling Force Pulsation. *Journal of Engineering for Industry*, 1994. https://doi.org/10.1115/1.2901804

[7] Jiunn-jyh Junz, C.M. Wang, Zheng. Online identification of shearing and plowing constants in end milling. *Journal of Manufacturing Science and Engineering-transactions of The ASME*, 2003. https://doi.org/10.1115/1.1536931

[8] Zheng Li, Steven Y. Liang, Shreyes N. Melkote. Angle Domain Analytical Model for End Milling Forces. *Journal of Manufacturing Science and Engineering-transactions of The ASME*, 1998. https://doi.org/10.1115/1.2830121

[9] G. Yucesan and Y. Altintas. Prediction of ball end milling forces. *ASME Journal of Engineering for Industry*, 118(1):95–103, February 1996.

[10] E. J. A. Armarego and M. Uthaichaya. A mechanics of cutting approach for force prediction in turning operations. *Journal of Engineering Production*, 1(1):1–18, 1977.

[11] E. Budak and Y. Altıntaş. Prediction of milling force coefficients from orthogonal cutting data. *Journal of Manufacturing Science and Engineering*, 118(2):216–224, 1996.

[12] M. R. Movahhedy, M. S. Gadala, and Y. Altintas. Simulation of the orthogonal metal cutting process using an arbitrary Lagrangian–Eulerian finite-element method. *Journal of Materials Processing Technology*, 103(2):267–275, 2000. 10.1016/S0924-0136(00)00488-9.

[13] Q. Zhu, W. Zeng, and J. Wang. Milling force prediction in high-speed milling of titanium alloy using deep learning approach. *Journal of Manufacturing Processes*, 45:746–753, 2019. 10.1016/j.jmapro.2019.08.025.

[14] A. M. Khan, V. Agrawal, and M. K. Gupta. Intelligent models for prediction of cutting forces in high-speed milling of Inconel 718 alloy. *Materials Today: Proceedings*, 28:1365–1370, 2020. 10.1016/j.matpr.2020.03.126.

[15] J. F. Kakkassery and S. Uthayakumar. Estimation of cutting force based on multi-sensorial data. Master's thesis, Chalmers University of Technology, 2021.

[16] P. Albertelli, M. Goletti, M. Torta, M. Salehi, and M. Monno. Model-based broadband estimation of cutting forces and tool vibration in milling through in-process indirect multiple-sensors measurements. *International Journal of Advanced Manufacturing Technology*, June 2015.

[17] K. Kiran and M. C. Kayacan. Cutting force modeling and accurate measurement in milling of flexible workpieces. *Mechanical Systems and Signal Processing*, 133:106284, 2019. 10.1016/j.ymssp.2019.106284.

[18] Y. Altıntaş, S. S. Park. Dynamic Compensation of Spindle-Integrated Force Sensors. *International Journal of Machine Tools and Manufacture*, 44(11):1179-1187, 2004.

[19] Q. Li, M. Hou, and H. Cao. Online identification of milling forces using acceleration signals. *The International Journal of Advanced Manufacturing Technology*, 127:1–11, 2023. 10.1007/s00170-023-11645-1.

[20] C. Wang, X. Zhang, B. Qiao, X. Chen, H. Cao. Milling force identification from acceleration signals using regularization method based on TSVD in peripheral milling. *Procedia CIRP*, 77:18–21, 2018.

[21] J. Zhou, X. Mao, H. Liu, B. Li, and Y. Peng. Prediction of cutting force in milling process using vibration signals of machine tool. *The International Journal of Advanced Manufacturing Technology*, 99:1–10, 2018. 10.1007/s00170-018-2464-1.

[22] R. Patil and S. Gombi. Prediction of cutting forces experimentally in end milling process using inverse analysis. *IOP Conference Series: Materials Science and Engineering*, 577:012177, 2019. 10.1088/1757-899X/577/1/012177.

[23] M.M. Joddar, K. Ahmadi. Estimating Milling Forces from Vibration Measurements. *Journal of Engineering for Industry*, 121(4):586-589, 1999.

[24] B. Powałka, J. S. Dhupia, A. Galip, U. Reuven, K. Katz. Identification of machining force model parameters from acceleration measurements. *International Journal of Manufacturing Research*, 2008.

[25] J. Kouguchi, H. Yoshioka. Monitoring method of cutting forces and vibrations by using frequency separation of acceleration sensor signals during milling process with small ball end mills. *Precision Engineering*, 85:337-356, 2024.

[26] B.-C. Shin, S.-J. Ha, M.-W. Cho, T.-I. Seo, G.-S. Yoon, Y.-M. Heo. Indirect cutting force measurement in the micro end-milling process based on frequency analysis of sensor signals. *Proceedings of the Institution of Mechanical Engineers, Part B: Journal of Engineering Manufacture*, 227(9):1341-1351, 2013.

[27] J. Tlusty and P. MacNeiL. Dynamics of cutting forces in end milling. *CIRP Annals*, 24:21, 1975.

[28] H. J. Fu, R. E. DeVor, and S. G. Kapoor. A mechanistic model for the prediction of the force system in face milling operation. *ASME Journal of Engineering for Industry*, 106:81, 1984.

[29] Y. Altıntaş. *Manufacturing Automation: Metal Cutting Mechanics, Machine Tool Vibrations, and CNC Design* (2nd ed.). Cambridge University Press, 2012.

[30] Y. Karpat and E. Budak. A new approach to predict cutting forces in milling. *International Journal of Machine Tools and Manufacture*, 51(2):131–142, 2011.

[31] Ş. Engin. Mechanics and dynamics of milling with generalized geometry. *PhD Thesis, Istanbul Technical University*, 2021. https://polen.itu.edu.tr/items/90d9ba93-fb2a-432e-b614-966bcbc88abb.

[32] R. G. Brown, P. Y. C. Hwang. *Introduction to Random Signals and Applied Kalman Filtering With Matlab* (4th ed.). Wiley, Hoboken, NJ, 2012.